TABLE 2. Summary of Analysis of LR Malformation in 18.5 Embroys from the Crosses between ActRIIB$^{+/-}$Smad2$^{+/-}$ and ActRIIB$^{-/-}$

ActRIIB$^{+/-}$Smad2$^{+/-}$ × ActRIIB$^{-/-}$							
		Thoracic heterotaxy					
Genotype			Cardiac defects				
ActRIIB	Smad2	-	-	PRPI	CRPI	Total	9 Rib
+/-	wt	26				25	
+/-	+/-	19(2)	3(1)			22	3
-/-	wt	10	2	6	8	26	26
-/-	+/-			1	13	14	14
total		55	5	7	21	88	

Total litters, 14; average pups/litter, 6.3; LR, left-right; PRPI, partial right pulmonary isomerism; CRPI, complete right pulmonary isomerism

a stomach in the thoracic cavity, agenesis of the spleen, and hypoplasia of the kidney in addition to hypoplasia of the pancreas (Fig. 3E). The functional unit of the endocrine pancreas is the islet of Langerhans, which are nested within the exocrine tissue of the pancreas and are composed of α, β-, δ-, and PP-cells. Pancreas β-cells produce insulin and form the core of the islet, whereas α-, δ-, and PP-cells are arranged at the periphery of the islet and secrete glucagon, somatostatin, and a pancreatic polypeptide, respectively. Histology of the pancreas revealed that the islets were nested in the wild-type embryo as shown in Figure 3B,D, whereas the islets of ActRIIB$^{-/-}$Smad2$^{+/-}$ embryo did not form round-shapes, but instead formed linear- or bundle-shapes as shown in Figure 3F,H. Immunohistochemical (IHC) studies revealed that the insulin-positive cells were significantly reduced in ActRIIB$^{-/-}$Smad2$^{+/-}$ embryo (Fig. 3G), consistent with the reduction in pancreatic insulin content (Fig. 2B). In rodent islets, there is a clear segregation of cell types to different regions of the islet as mentioned above. We thus examined this segregation of endocrine cells in islets by IHC. In wild-type mice, insulin positive β-cells were clustered in the core of the round-shaped islet (Fig. 3I,L) and glucagon-positive a-cell were peripherally located in a mantle shape (Fig. 3J,L), consistent with the description in textbook. In the ActRIIB$^{-/-}$Smad2$^{+/-}$ embryo, the insulin positive β-cells were nested but also lined up along the bundle-shape islets and the glucagon-positive α-cells were arranged at the periphery of the linear- or bundle-shape islets (Fig. 3M,N,P). The pancreatic polypeptide-positive PP-cells were also detected at the periphery of the islets in the wild-type pancreas (Fig. 3K). In striking contrast, pancreatic polypeptide-positive cells could not be detected in the ActRIIB$^{-/-}$Smad2$^{+/-}$ pancreata (Fig. 3O), indicating that the differentiation of PP cells was severely impaired in the ActRIIB$^{-/-}$Smad2$^{+/-}$ islet. To address the gene dosage effect of ActRIIB and Smad2 on the differentiation of PP cells, IHC with PP antibody was performed in the Smad2$^{+/-}$ and the ActRIIB$^{+/-}$Smad2$^{+/-}$ pancreata. The PP-positive cells were clearly detected at the periphery of the round-shaped islets in both the Smad2$^{+/-}$ and the ActRIIB$^{+/-}$Smad2$^{+/-}$ mutant pancreases as in the wild-type pancreas (data not shown), suggesting that β-cell differentiation is more sensitive to loss-of-function mutations in ActRIIB and Smad2 than PP-cell differentiation. Taken together, our results strongly suggest that the ActRIIB-Smad2 signal is essential for the endocrine cell linage development in the pancreas islets.

Impaired Glucose-Induced Insulin Secretion in Adult ActRIIB/Smad2 Mutant Mice

We next analyzed the glucose metabolism in ActRIIB$^{+/-}$Smad2$^{+/-}$, Smad2$^{+/-}$, ActRIIB$^{+/-}$, and wild-type mice. Mice were fed a normal laboratory chow diet. Although blood glucose and insulin levels after an overnight fast in

Fig. 1. Right pulmonary isomerism and cardiac outflow tract anomalies in ActRIIB$^{-/-}$Smad2$^{+/-}$ newborn mice. A,B: Ventral view of the wild-type and the ActRIIB$^{-/-}$Smad2$^{+/-}$ lungs. **A:** The wild-type lungs have four right lobes and one left lobe. **B:** In the mutant mice, both right and left lungs have four lobes in mirror image. **C:** Right-side view of the mutant mouse with the stomach (arrow) in the thoracic region. D–F: Ventral view of the wild-type (D) and the mutant hearts (E,F). **D:** In the wild-type heart, the pulmonary trunk (PT) is located anterior to the aorta (Ao) and crosses over to the left of the Ao. **E:** In the mutant heart, the Ao arise from the anterior-most position of the heart, whereas the PT was located posterior to, and on the right side of, the Ao. **F:** In the mutant heart, the descending Ao loops to the right side, instead of looping to the left as in the wild-type mice. crl, cranial lobe; ml, medial lobe; cal, caudal lobe; al, accessory lobe; LL, left lung; HE, heart; st, stomach; dp, diaphragm; aAo, ascending aorta; dAo, descending aorta.

Fig. 3. Defective islet formation in the ActRIIB$^{-/-}$Smad2$^{+/-}$ embryo. Upper and lower panels show wild-type and ActRIIB$^{-/-}$Smad2$^{+/-}$ mouse, respectively. **A,E:** Sagittal sections of the embryos revealed mislocation of the pancreas (outlined by dashes) and stomach (asterisk) in ActRIIB$^{-/-}$Smad2$^{+/-}$embryo. **B,D,F,H:** Hematoxylin and eosin (HE) staining of the pancreas. In the wild-type pancreata (B,D), round-shaped isles (surrounded by arrowheads) were observed, whereas linear-shaped islets (indicated by arrowheads) were observed in the mutant pancreases (F,H). **C,G:** Immunostaining for insulin in serial sections of B and F, respectively. **I–K,M–O:** The serial sections of wild-type and ActRIIB$^{-/-}$Smad2$^{+/-}$ pancreata were immunostained for insulin (I,M), glucagon (J,N), and pancreatic polypeptide (K,O), respectively. **L,P:** Immunofluorescence staining for insulin (red) and glucagon (green). Scale bars = 100 μm.

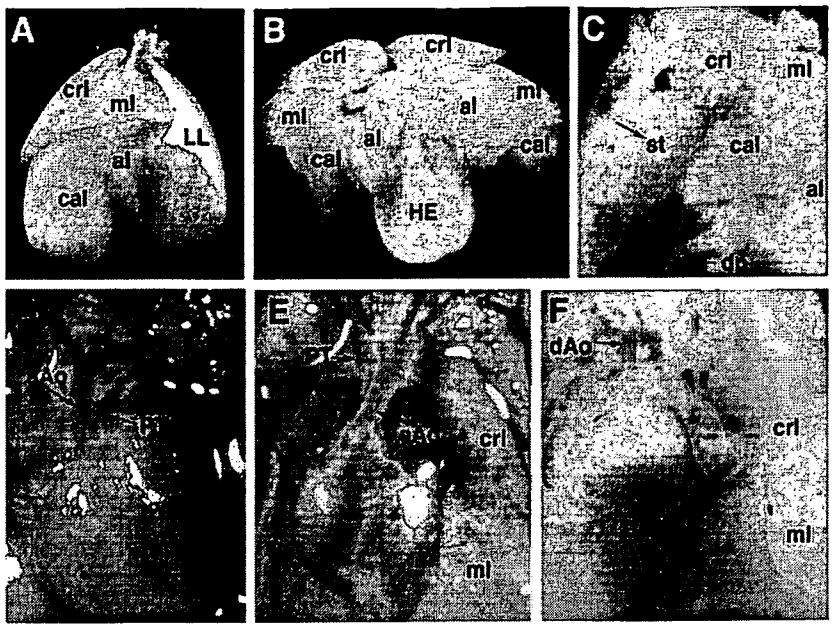

Fig. 1.

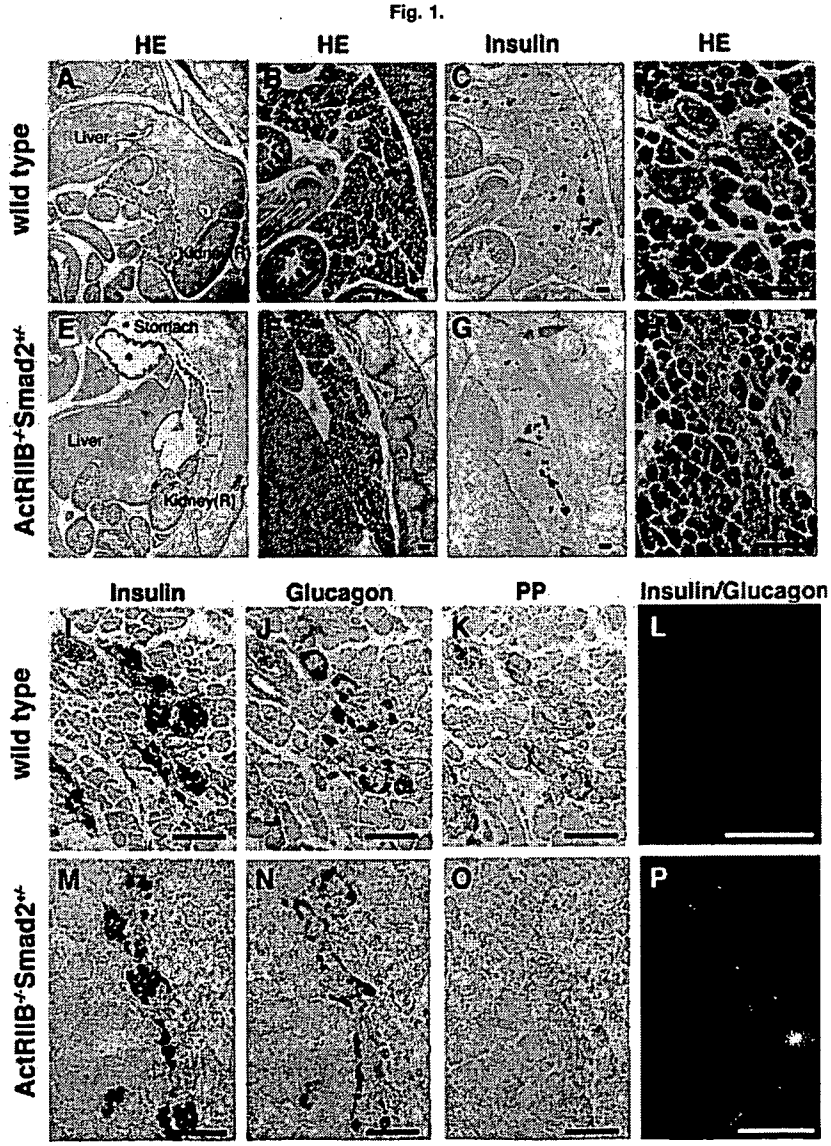

Fig. 3.

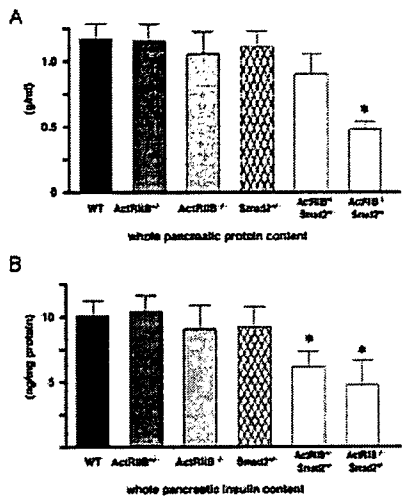

Fig. 2. Pancreas weight and insulin content in the embryos. **A:** The embryos from the crosses between ActRIIB$^{+/-}$Smad2$^{+/-}$ and ActRIIB$^{+/-}$ mice were analyzed before birth at embryonic day (e) 18.5. The pancreases were dissected out and weighed. *$P < 0.01$ for ActRIIB$^{-/-}$Smad2$^{+/-}$ vs. the others without an asterisk. **B:** Whole pancreatic insulin contents were measured after acid–ethanol extraction. *$P < 0.01$ for ActRIIB+/−Smad2$^{+/-}$ and ActRIIB$^{-/-}$Smad2$^{+/-}$ vs. the others without an asterisk. At least three embryos were analyzed in each group. Data presented as average ± standard error of the mean (SEM).

these mutant mice appeared similar to those of their wild-type littermates, ActRIIB$^{+/-}$Smad2$^{+/-}$ and Smad2$^{+/-}$ mice exhibited impaired glucose tolerance during an intrapertoneal glucose-tolerance test (Fig. 4A). In glucose tolerance tests after an overnight fast, ActRIIB$^{+/-}$Smad2$^{+/-}$ mice had abnormal peak glucose levels, and prolonged hyperglycemia. Smad2$^{+/-}$ mice also exhibited a prolonged ensuing hyperglycemia, although there was no significant difference in a peak glucose levels. It is noted that ActRIIB$^{+/-}$ mice exhibited normal glucose handling, consisting with a previous report (Kim et al., 2000), whereas a lack of one allele of Smad2 on the background of ActRIIB$^{+/-}$ resulted in a dramatic worsening of glucose tolerance. We then measured insulin levels in these mice after an overnight fast, and they were similar in ActRIIB$^{+/-}$Smad2$^{+/-}$, Smad2$^{+/-}$, and wild-type animals. Insulin levels were reduced inappropriately, however, in ActRIIB$^{+/-}$Smad2$^{+/-}$ and Smad2$^{+/-}$ animals after glucose challenge (Fig. 4B), suggesting that the observed impairment in glu-

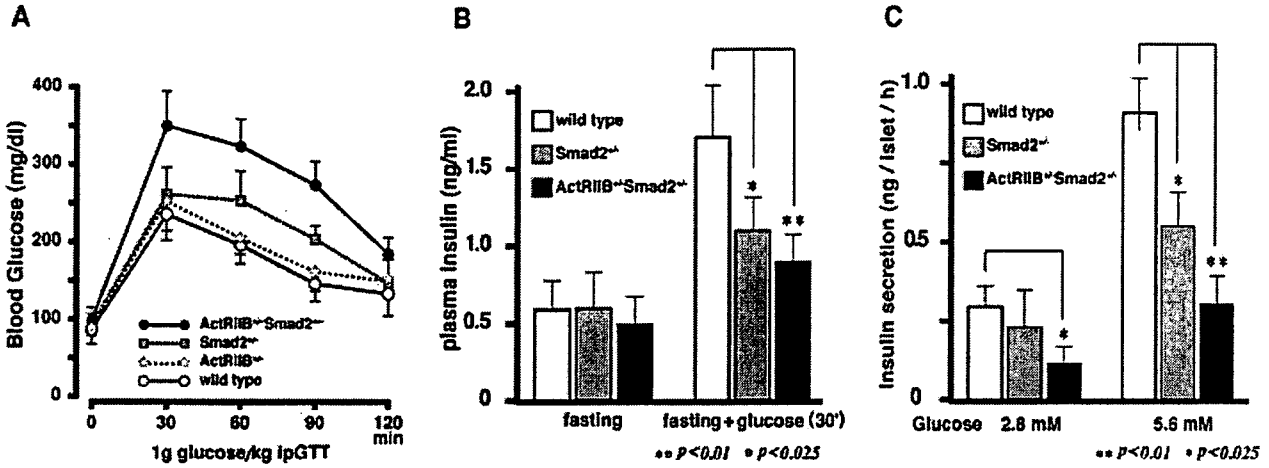

Fig. 4. Defective glucose-stimulated insulin secretion. **A:** Glucose tolerance testing of 12- to 16-week-old male mice (n = 6 per group). **B:** Insulin levels during the ipGTT at 30 min after glucose injection. **C:** Glucose-stimulated insulin secretion from isolated islets. Insulin secretion was assessed in triplicate in each group. Data presented as average ± standard error of the mean (SEM).

cose tolerance may result from inadequate insulin production or secretion. To further define the effects of the genetic defects on glucose-induced insulin secretion, islets were isolated from ActRIIB$^{+/-}$Smad2$^{+/-}$, Smad2$^{+/-}$ and wild-type animals and the changes in glucose-stimulated insulin secretion were analyzed. Consistent with the glucose tolerance test, the changes in the insulin secretary response to glucose in ActRIIB$^{+/-}$Smad2$^{+/-}$ islets was profoundly lower than that of wild-type islets, particularly at higher glucose concentrations (Fig. 4C).

Islet Hypoplasia in ActRIIB$^{+/-}$ Smad2$^{+/-}$ Mice

Inactivation of ActRIIB and Smad2 in adult mice resulted in pancreas islet hypoplasia (Fig. 5A,B). Histologic and morphometric analysis of pancreas islet in ActRIIB$^{+/-}$Smad2$^{+/-}$ and Smad2$^{+/-}$ animals revealed a significantly reduced islet size in these animals (Fig. 5A). Average islet size in wild-type animals is 14,900 ± 5,700 μm^2, in Smad2$^{+/-}$ is 9,400 ± 860 μm^2, and in ActRIIB$^{+/-}$Smad2$^{+/-}$ is 6,700 ± 700 μm^2. Distribution of islet areas <5,000 μm^2, 5,000–10,000 μm^2, 10,000–15,000 μm^2, or >15,000 μm^2 is shown in Figure 5B as a percentage of islets measured. As shown in Figure 5B, islet size in Smad2$^{+/-}$ and ActRIIB$^{+/-}$Smad2$^{+/-}$ is reduced. There was an increased proportion of small islets and a decreased proportion of large islets in the mutant mice. In contrast, the islet size in ActRIIB$^{+/-}$ mice was not significantly reduced. There was a significant reduction of insulin content in ActRIIB$^{+/-}$Smad2$^{+/-}$ mice, reflecting the islet hypoplasia in the histology of ActRIIB$^{+/-}$Smad2$^{+/-}$ mice. We next examined the segregation of endocrine cells in islets by immunohistochemistry. In ActRIIB$^{+/-}$Smad2$^{+/-}$ mice, β-cells were clustered in the core of round islet and α cell located peripherally in a mantle shape as shown in Figure 5D, indicating that islet architecture was not affected by the compound hetero mutation of ActRIIB and Smad2, which resulted in islet hypoplasia. These results suggest that the endocrine pancreas is particularly sensitive to the gene dosage of ActRIIB and Smad2 and the trans-heterozygous ActRIIB$^{+/-}$Smad2$^{+/-}$ mice may thus provide a polygenic animal model of impaired glucose tolerance.

DISCUSSION

To investigate the genetic interaction of ActRIIB and Smad2, we bred ActRIIB$^{+/-}$Smad2$^{+/-}$ mice with either ActRIIB$^{-/-}$ or ActRIIB$^{+/-}$ mice on a 129/SVJ/C57BL6 hybrid background and compared the phenotypes among the littermates. In this study, we provided genetic evidence that ActRIIB interacts with Smad2 not only in determination of left–right patterning of the thoracic organs but also in pancreas islet development.

We found that, without exception, the mice with the ActRIIB$^{-/-}$ Smad2$^{+/-}$ genotype died perinatally with complete penetrance of cardiac malformations and the right pulmonary isomerism. In addition, these left–right patterning defects were newly emerged in some of the ActRIIB$^{+/-}$Smad2$^{+/-}$ mice. Genetic crosses of nodal, a member of the TGF-β family, and Smad2 knockout mice in the previous study demonstrated a strong phenocopy of ActRIIB-Smad2 phenotypes of left–right patterning in the nodal/Smad2 compound heterozygous mice (Nomura and Li, 1998). The emergence of such identical phenotypes may suggest that nodal signals through ActRIIB and Smad2 regulate these patterning events during mouse development. This hypothesis is further supported by the evidence that nodal signals through ActRIIB in association with the coreceptor Cripto and ActRIB activate Smad2 phosphorylation using a *Xenopus* embryo assay system (Yeo and Whitman, 2001).

The TGF-β family is a major regulator of pancreatic endocrine and exocrine cell fate in the pancreas. The components in the TGF-β signaling pathway, including the TGF-β ligands activin and TGF-β1, their respective receptors, ligand antagonists including follistatin and noggin, and intracellular Smads such as Smad2 and

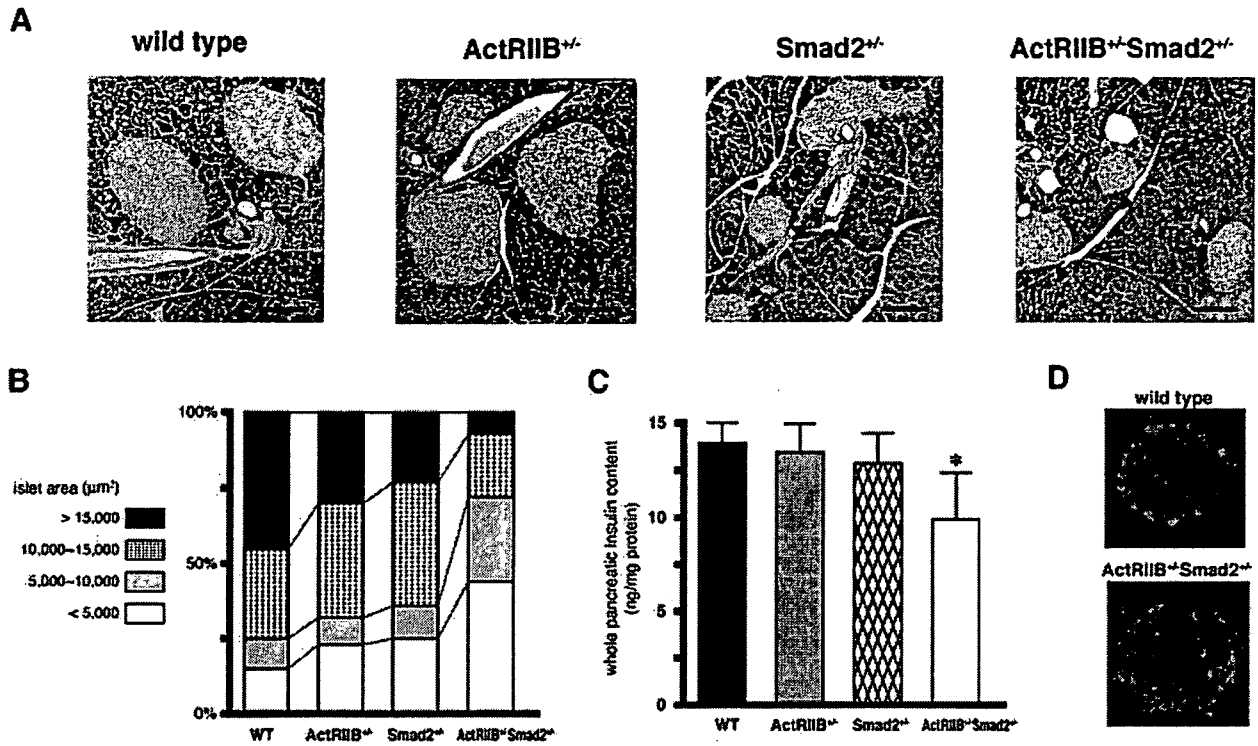

Fig. 5. Pancreas morphology and insulin contents in adult ActRIIB/Smad2 mutants. **A:** Representative photographs showing islet hypoplasia in $Smad2^{+/-}$ heterozygote and $ActRIIB^{+/-}Smad2^{+/-}$ compound heterozygote. Tissues were stained by hematoxylin and eosin (HE). Islets (arrowheads) from wild-type, $ActRIIB^{+/-}$, $Smad2^{+/-}$, and $ActRIIB^{+/-}Smad2^{+/-}$ adults. **B:** Morphometric analysis of islet area in pancreata from wild-type and mutant adults. For wild-type, n = 219; $ActRIIB^{+/-}$, n = 189; $Smad2^{+/-}$, n = 207; $ActRIIB^{+/-}Smad2^{+/-}$, n = 219. Distribution of islet areas <5,000, 5,000–10,000, 10,000–15,000 or >15,000 μm^2 is shown as a percentage of islets measured. $P < 0.001$ for wild-type vs. $ActRIIB^{+/-}Smad2^{+/-}$ and $P < 0.05$ for wild-type vs. $Smad2^{+/-}$. Data are presented as means ± standard error of the mean (SEM). **C:** Insulin content in whole pancreases from the mice in each group. $^*P < 0.01$ for $ActRIIB^{+/-}Smad2^{+/-}$ vs. the others without asterisk. **D:** Immunofluorescence staining for insulin (red) and glucagon (green), showing normal islet architecture in $ActRIIB^{+/-}Smad2^{+/-}$ mutant. Scale bars = 100 μm in A.

Smad4, are expressed in the embryonic pancreas epithelium and mesenchyme (Ogawa et al., 1993; Feijen et al., 1994; Furukawa et al., 1995; Manova et al., 1995; Verschueren et al., 1995; Crisera et al., 2000; Tremblay et al., 2000), suggesting not only the importance but also the complexity of the TGF-β system in pancreas development. In vitro exposure of the embryonic mouse pancreas to TGF-β1 or activin promotes development of endocrine cells, particularly β-cells and PP cells (Sanvito et al., 1994), and disrupts epithelial branching and acinar formation (Ritvos et al., 1995). Moreover, follistatin, a known antagonist of activins, promotes embryonic exocrine cell differentiation and reduces differentiation of endocrine cells (Miralles et al., 1998). These in vitro observations suggest that TGF-β family ligands, including activin and TGF-β1, may promote endocrine cell development. A recent study by Kim and colleagues provided strong genetic evidence that another TGF-β family member, GDF11, regulates both the production of pancreatic islet progenitor cells and the maturation of these progenitor cells into insulin-producing β-cells. In $GDF11^{-/-}$ mice, the number of islet precursor cells was increased, whereas that of insulin-producing cells was reduced, resulting in islet hypoplasia. In addition, they found a similar phenotype in islets of $Smad2^{+/-}$ mice, suggesting that GDF11 and Smad2 function in the same signaling pathway to regulate islet development. In this study, we have provided genetic evidence for the gene dosage requirement of ActRIIB and Smad2 on islet formation. Inactivation of ActRIIB and Smad2 in mice resulted in pancreatic islet hypoplasia, supporting the hypothesis that GDF11 signaling uses the activin receptor-Smad2 system as cellular components to regulate pancreas islet development. However, the precise comparison of the islet phenotype between $GDF11^{-/-}$ and ActRIIB/Smad2 compound mutant mice shown in this study revealed the complexity of TGF-β signaling in pancreatic islet development. In $ActRIIB^{-/-}Smad2^{+/-}$ mice, glucagon-positive cells (a-cells) were produced and their amount was comparable to that in wild-type mice (Fig. 3J,N), whereas the amount of α-cells in $GDF11^{-/-}$ mice was significantly increased, suggesting that GDF11 may negatively regulate α-cells differentiation by using a signaling pathway independent of ActRIIB-Smad2 system. In $ActRIIB^{-/-}Smad2^{+/-}$ mice, pancreatic polypeptide producing PP-cells were hardly detected, together with a significant reduction of insulin-producing β-cells, which may be consistent with a previous in vitro observation that TGF-β1 promoted the differentiation of endocrine cells in pancreas bud culture, particularly of those containing the pancreatic polypeptide and insulin (Sanvito et al., 1994). On

the other hand, the PP-cells were normally detected in GDF11$^{-/-}$ mice, indicating that GDF11 is dispensable for PP-cell differentiation. The other TGF-β ligands like activins may signal through ActRIIB-Smad2 to positively regulate PP-cell differentiation. Moreover, we found abnormal islet morphology and hypoplastic pancreas in ActRIIB$^{-/-}$Smad2$^{+/-}$ mice. Although we could not rule out the possibility that changes in islet morphology and pancreas size in ActRIIB$^{-/-}$Smad2$^{+/-}$ mice were secondary to axial patterning defects, the reduction in insulin content and pancreas size in the mutant pancreas suggest important roles of ActRIIB and Smad2 signal(s) not only in endocrine cells differentiation but also in exocrine cell differentiation. Collectively, TGF-β signaling through ActRIIB and Smad2 is an important determinant for endocrine cell fate and plays critical roles in orchestrated developmental process of pancreas.

We further demonstrated the gene dosage effect of ActRIIB and Smad2 in glucose-responsive insulin secretion in the adult mice. Both ActRIIB$^{+/-}$ Smad2$^{+/-}$ and Smad2$^{+/-}$ mice exhibited impaired glucose tolerance on ipGTT. It should be noted that isolated islets from the mutant mice also exhibited impaired insulin secretion on glucose stimulation, suggesting that the signaling through ActRIIB and Smad2 is essential in islet β-cells for efficient glucose-responsive insulin secretion. Pancreatic β-cell–specific gene ablation will be required to further determine the roles of ActRIIB and Smad2 in glucose-responsive insulin secretion. Although no evidence for linkage in ActRIIB with type II diabetes was observed in a French Caucasian population (Dupont et al., 2001), our results raise the question of whether Smad2 or ActRIIB is one of the susceptibility genes for pandemic type II diabetes that is known as a polygene disease.

EXPERIMENTAL PROCEDURES

Mice and Crosses

Detailed procedures for the generation of ActRIIB and Smad2 knockout mice are described elsewhere (Oh and Li, 1997; Nomura and Li, 1998). ActRIIB$^{+/-}$ mice were crossed with Smad2$^{+/-}$ mice on a 129SV/C57BL6 hybrid background. Compound heterozygous ActRIIB$^{+/-}$Smad2$^{+/-}$ mice were viable and fertile. Male ActRIIB$^{-/-}$ or ActRIIB$^{+/-}$ mice were mated with female ActRIIB$^{+/-}$ Smad2$^{+/-}$ mice and newborn pups or e18.5 fetuses were collected. Anatomic abnormalities of these mice were observed under the dissection microscope as described below. Genotypes of individual pups were performed by Southern blot analysis. All animal experiments were approved by the animal care and use committee of Kyushu University School of Medicine.

Anatomic Analysis of Laterality Defects in Heart and Lung

The criteria for cardiac defects and right pulmonary isomerism used in this study were previously described (Oh and Li, 1997; Oh et al., 2002). Briefly, outflow tract defects were recognized when the ascending Ao was placed anterior to the pulmonary trunk (PT). The PT is normally located anterior to and to the right of the Ao and crosses over to the left of the Ao. However, in the mutant mice, the Ao arose from the anterior-most position of the heart, where the PT was located in the wild-type, whereas the PT was located posterior to, and on either the left or the right side of the Ao, and the PT and the Ao were in parallel positions without crossing over each other. These abnormalities of the outflow tract are similar to the human congenital heart defects known as TGA or DORV. In normal mice, the lung consists of four right lobes and one large left lobe, whereas the left lung in complete RPI or incomplete RPI consists of four or three lobes, respectively.

Histological Analysis

The animals were killed by decapitation after an overnight fast. The whole pancreas was excised, weighed, and cut into two pieces corresponding to the head (duodenal) and the tail (spleen) parts of the organ. The tissues were separately fixed in 4% paraformaldehyde, dehydrated in 100% ethanol, and embedded in paraffin. Each entire pancreatic piece was cut, through its length, into 5-mm-thick sections. Every 30th section of each pancreas piece was stained with hematoxylin and eosin, yielding 11 sections per animal.

The embryos were collected at e18.5 and fixed in 4% paraformaldehyde, dehydrated, and embedded in paraffin. Immunohistochemistry was performed as described (Hashimoto et al., 2005). For immunostaining, sections were subjected to antigen retrieval using DAKO Cytomation Target Retrieval Solution (Dako Corporation, Carpinteria, CA). After blocking by BlockAce (Dainippon Sumitomo Pharmaceutical Co. Ltd., Osaka, Japan), sections were incubated with primary antibodies at 4°C for 12–16 hr, followed by 1-hr incubation with secondary antibodies. Guinea pig anti-porcine insulin antibody (1:500), rabbit anti-human glucagon antibody (1:500), and rabbit anti-human pancreatic polypeptide antibody (1:600; Dako Corporation) were used as the primary antibodies. Alexa Fluor 594-conjugated goat anti-guinea pig IgG and Alexa Fluor 488-conjugated donkey anti-rabbit IgG (Molecular Probes, Eugene, OR) were used as the secondary antibodies for insulin and glucagon, respectively. Immunofluorescencewas viewed under laser microscopy BioZero (Keyence, Osaka, Japan).

Morphometry Measurements

The pancreatic tissue area was determined by computer-assisted measurements using a Keyence BioZero microscope. The area of each pancreatic islet was measured, and the data were subjected to statistical analysis using Excel (Microsoft). The islets less than 5,000 μm^2 in area were defined as small; those ranging 5,000–15,000 μm^2 as medium and those exceeding 15,000 μm^2 as large.

Glucose Tolerance Tests and Insulin Content

To assess glucose tolerance, adult (12–16 weeks old) mice were fasted overnight and we measured baseline blood glucose levels in tail-vein blood using a Glutest Sensor (Sanwa Kagaku Inc., Nagoya, Japan). Glucose (1 mg dextrose/g body weight) in sterile phosphate buffered saline was in-

jected intraperitoneally, and blood glucose levels were measured 30, 60, 90, and 120 min after injection. To measure plasma insulin levels, ~50 μl of blood was collected from the tail vein before and 30 min after intraperitoneal injection with glucose. Blood samples were centrifuged, and serum was used to measure insulin concentrations. The insulin content of whole pancreas was determined after extraction with acid–ethanol. Insulin levels were detected using a rat/mouse insulin ELISA kit (Morinaga Institute of Biological Science Inc., Kanagawa, Japan).

Insulin Secretion in Isolated Islets

Pancreatic islets of adult nonfasted ActRIIB$^{+/-}$Smad2$^{+/-}$, Smad2$^{+/-}$, and wild-type male mice (4–6 months old) were isolated, as described (Lacy and Kostianovsky, 1967), using digestion with collagenase type IV (Worthington Biochemical Corp., NJ). In brief, mice were killed, and collagenase in Hanks' solution (24020-117, Gibco, Invitrogen, Carlsbad, CA) was injected into the billiary tract. Then, the pancreas was excised and incubated for 15 min at 37°C. After incubation and agitation, the suspension was transferred to centrifuge tubes in Hanks' solution and washed three times by centrifugation for 1 min at 1,000 rpm. Then, islets were obtained by density gradient with HISTOPAQE-1077 and -1119 (Sigma, Tokyo, Japan) and picked under a stereomicroscope. The isolated islets were cultured in RPMI1640 medium (R5787, Sigma) containing 10% fetal bovine serum with 37°C, 5% CO_2 incubator for 48 hr. Insulin secretion from the isolated islets was measured over a period of 30 min, in Krebs–Ringer bicarbonate-4-(2-hydroxyethyl)-1-piperazine ethanesulfonic acid (HEPES) buffer (KRB; 140 mM NaCl, 3.6 mM KCl, 0.5 mM NaH_2PO_4, 0.5 mM $MgSO_4$, 1.5 mM $CaCl_2$, 2 mM $NaHCO_3$, 10 mM HEPES, and 0.1% bovine serum albumin), containing 2.8 or 5.6 mM glucose. Insulin levels were detected using a rat/mouse insulin ELISA kit (Morinaga Institute of Biological Science Inc.).

Statistical Analysis

In all cases, differences among sample means were assessed by analysis of variance followed by the Newman–Keuls test of multiple comparisons. A P value less than 0.05 was considered statistically significant.

ACKNOWLEDGMENTS

We thank L. Hong, Y. Lian, and Y. Hamaguchi for expert assistance. The work of Dr. M.N. was supported by grant from Takeda science foundation.

REFERENCES

Attisano L, Wrana JL, Cheifetz S, Massague J. 1992. Novel activin receptors: distinct genes and alternative mRNA splicing generate a repertoire of serine/threonine kinase receptors. Cell 68:97–108.

Crisera CA, Maldonado TS, Kadison AS, Li M, Alkasab SL, Longaker MT, Gittes GK. 2000. Transforming growth factor-beta 1 in the developing mouse pancreas: a potential regulator of exocrine differentiation. Differentiation 65:255–259.

Derynck R, Feng XH. 1997. TGF-βeta receptor signaling. Biochim Biophys Acta 1333:F105–F150.

Dupont S, Hani EH, Cras-Meneur C, De Matos F, Lobbens S, Lecoeur C, Vaxillaire M, Scharfmann R, Froguel P. 2001. No evidence for linkage or for diabetes-associated mutations in the activin type 2B receptor gene (ACVR2B) in French patients with mature-onset diabetes of the young or type 2 diabetes. Diabetes 50:1219–1221.

Feijen A, Goumans MJ, van den Eijnden-van Raaij AJ. 1994. Expression of activin subunits, activin receptors and follistatin in postimplantation mouse embryos suggests specific developmental functions for different activins. Development 120:3621–3637.

Furukawa M, Eto Y, Kojima I. 1995. Expression of immunoreactive activin A in fetal rat pancreas. Endocr J 42:63–68.

Harmon EB, Apelqvist AA, Smart NG, Gu X, Osborne DH, Kim SK. 2004. GDF11 modulates NGN3+ islet progenitor cell number and promotes beta-cell differentiation in pancreas development. Development 131:6163–6174.

Hashimoto N, Kido Y, Uchida T, Matsuda T, Suzuki K, Inoue H, Matsumoto M, Ogawa W, Maeda S, Fujihara H, Ueta Y, Uchiyama Y, Akimoto K, Ohno S, Noda T, Kasuga M. 2005. PKClambda regulates glucose-induced insulin secretion through modulation of gene expression in pancreatic beta cells. J Clin Invest 115:138–145.

Heldin CH, Miyazono K, ten Dijke P. 1997. TGF-βeta signalling from cell membrane to nucleus through SMAD proteins. Nature 390:465–471.

Kim SK, Hebrok M, Li E, Oh SP, Schrewe H, Harmon EB, Lee JS, Melton DA. 2000. Activin receptor patterning of foregut organogenesis. Genes Dev 14:1866–1871.

Lacy PE, Kostianovsky M. 1967. Method for the isolation of intact islets of Langerhans from the rat pancreas. Diabetes 16:35–39.

Lee SJ, McPherron AC. 2001. Regulation of myostatin activity and muscle growth. Proc Natl Acad Sci U S A 98:9306–9311.

Manova K, De Leon V, Angeles M, Kalantry S, Giarre M, Attisano L, Wrana J, Bachvarova RF. 1995. mRNAs for activin receptors II and IIB are expressed in mouse oocytes and in the epiblast of pregastrula and gastrula stage mouse embryos. Mech Dev 49:3–11.

Massague J, Chen YG. 2000. Controlling TGF-βeta signaling. Genes Dev 14:627–644.

Mathews LS. 1994. Activin receptors and cellular signaling by the receptor serine kinase family. Endocr Rev 15:310–325.

Matzuk MM, Kumar TR, Bradley A. 1995. Different phenotypes for mice deficient in either activins or activin receptor type II. Nature 374:356–360.

Miralles F, Czernichow P, Scharfmann R. 1998. Follistatin regulates the relative proportions of endocrine versus exocrine tissue during pancreatic development. Development 125:1017–1024.

Nomura M, Li E. 1998. Smad2 role in mesoderm formation, left-right patterning and craniofacial development. Nature 393:786–790.

Ogawa K, Abe K, Kurosawa N, Kurohmaru M, Sugino H, Takahashi M, Hayashi Y. 1993. Expression of alpha, beta A and beta B subunits of inhibin or activin and follistatin in rat pancreatic islets. FEBS Lett 319:217–220.

Oh SP, Li E. 1997. The signaling pathway mediated by the type IIB activin receptor controls axial patterning and lateral asymmetry in the mouse. Genes Dev 11:1812–1826.

Oh SP, Yeo CY, Lee Y, Schrewe H, Whitman M, Li E. 2002. Activin type IIA and IIB receptors mediate Gdf11 signaling in axial vertebral patterning. Genes Dev 16:2749–2754.

Ritvos O, Tuuri T, Eramaa M, Sainio K, Hilden K, Saxen L, Gilbert SF. 1995. Activin disrupts epithelial branching morphogenesis in developing glandular organs of the mouse. Mech Dev 50:229–245.

Sanvito F, Herrera PL, Huarte J, Nichols A, Montesano R, Orci L, Vassalli JD. 1994. TGF-βeta 1 influences the relative development of the exocrine and endocrine pancreas in vitro. Development 120:3451–3462.

Shiozaki S, Tajima T, Zhang YQ, Furukawa M, Nakazato Y, Kojima I. 1999. Impaired differentiation of endocrine and exocrine cells of the pancreas in transgenic mouse expressing the trun-

cated type II activin receptor. Biochim Biophys Acta 1450:1–11.

Song J, Oh SP, Schrewe H, Nomura M, Lei H, Okano M, Gridley T, Li E. 1999. The type II activin receptors are essential for egg cylinder growth, gastrulation, and rostral head development in mice. Dev Biol 213:157–169.

Tremblay KD, Hoodless PA, Bikoff EK, Robertson EJ. 2000. Formation of the definitive endoderm in mouse is a Smad2-dependent process. Development 127:3079–3090.

Venter JC, Adams MD, Myers EW, Li PW, Mural RJ, Sutton GG, Smith HO, Yandell M, Evans CA, Holt RA, Gocayne JD, Amanatides P, Ballew RM, Huson DH, Wortman JR, Zhang Q, Kodira CD, Zheng XH, Chen L, Skupski M, Subramanian G, Thomas PD, Zhang J, Gabor Miklos GL, Nelson C, Broder S, Clark AG, Nadeau J, McKusick VA, Zinder N, Levine AJ, Roberts RJ, Simon M, Slayman C, Hunkapiller M, Bolanos R, Delcher A, Dew I, Fasulo D, Flanigan M, Florea L, Halpern A, Hannenhalli S, Kravitz S, Levy S, Mobarry C, Reinert K, Remington K, Abu-Threideh J, Beasley E, Biddick K, Bonazzi V, Brandon R, Cargill M, Chandramouliswaran I, Charlab R, Chaturvedi K, Deng Z, Di Francesco V, Dunn P, Eilbeck K, Evangelista C, Gabrielian AE, Gan W, Ge W, Gong F, Gu Z, Guan P, Heiman TJ, Higgins ME, Ji RR, Ke Z, Ketchum KA, Lai Z, Lei Y, Li Z, Li J, Liang Y, Lin X, Lu F, Merkulov GV, Milshina N, Moore HM, Naik AK, Narayan VA, Neelam B, Nusskern D, Rusch DB, Salzberg S, Shao W, Shue B, Sun J, Wang Z, Wang A, Wang X, Wang J, Wei M, Wides R, Xiao C, Yan C, Yao A, Ye J, Zhan M, Zhang W, Zhang H, Zhao Q, Zheng L, Zhong F, Zhong W, Zhu S, Zhao S, Gilbert D, Baumhueter S, Spier G, Carter C, Cravchik A, Woodage T,Ali F, An H, Awe A, Baldwin D, Baden H, Barnstead M, Barrow I, Beeson K, Busam D, Carver A, Center A, Cheng ML, Curry L, Danaher S, Davenport L, Desilets R, Dietz S, Dodson K, Doup L, Ferriera S, Garg N, Gluecksmann A, Hart B, Haynes J, Haynes C, Heiner C, Hladun S, Hostin D, Houck J, Howland T, Ibegwam C, Johnson J, Kalush F, Kline L, Koduru S, Love A, Mann F, May D, McCawley S, McIntosh T, McMullen I, Moy M, Moy L, Murphy B, Nelson K, Pfannkoch C, Pratts E, Puri V, Qureshi H, Reardon M, Rodriguez R, Rogers YH, Romblad D, Ruhfel B, Scott R, Sitter C, Smallwood M, Stewart E, Strong R, Suh E, Thomas R, Tint NN, Tse S, Vech C, Wang G, Wetter J, Williams S, Williams M, Windsor S, Winn-Deen E, Wolfe K, Zaveri J, Zaveri K, Abril JF, Guigo R, Campbell MJ, Sjolander KV, Karlak B, Kejariwal A, Mi H, Lazareva B, Hatton T, Narechania A, Diemer K, Muruganujan A, Guo N, Sato S, Bafna V, Istrail S, Lippert R, Schwartz R, Walenz B, Yooseph S, Allen D, Basu A, Baxendale J, Blick L, Caminha M, Carnes-Stine J, Caulk P, Chiang YH, Coyne M, Dahlke C, Mays A, Dombroski M, Donnelly M, Ely D, Esparham S, Fosler C, Gire H, Glanowski S, Glasser K, Glodek A, Gorokhov M, Graham K, Gropman B, Harris M, Heil J, Henderson S, Hoover J, Jennings D, Jordan C, Jordan J, Kasha J, Kagan L, Kraft C, Levitsky A, Lewis M, Liu X, Lopez J, Ma D, Majoros W, McDaniel J, Murphy S, Newman M, Nguyen T, Nguyen N, Nodell M, Pan S, Peck J, Peterson M, Rowe W, Sanders R, Scott J, Simpson M, Smith T, Sprague A, Stockwell T, Turner R, Venter E, Wang M, Wen M, Wu D, Wu M, Xia A, Zandieh A, Zhu X. 2001. The sequence of the human genome. Science 291:1304–1351.

Verschueren K, Dewulf N, Goumans MJ, Lonnoy O, Feijen A, Grimsby S, Vandi Spiegle K, ten Dijke P, Moren A, Vanscheeuwijck P, Heldin CH, Miyazono K, Mummery C, Van Den Eijnden-Van Raaij J, Huylebroeck D. 1995. Expression of type I and type IB receptors for activin in midgestation mouse embryos suggests distinct functions in organogenesis. Mech Dev 52:109–123.

Yamaoka T, Idehara C, Yano M, Matsushita T, Yamada T, Ii S, Moritani M, Hata J, Sugino H, Noji S, Itakura M. 1998. Hypoplasia of pancreatic islets in transgenic mice expressing activin receptor mutants. J Clin Invest 102:294–301.

Yamashita H, ten Dijke P, Huylebroeck D, Sampath TK, Andries M, Smith JC, Heldin CH, Miyazono K. 1995. Osteogenic protein-1 binds to activin type II receptors and induces certain activin-like effects. J Cell Biol 130:217–226.

Yeo C, Whitman M. 2001. Nodal signals to Smads through Cripto-dependent and Cripto-independent mechanisms. Mol Cell 7:949–957.

Steroidogenic factor 1/adrenal 4 binding protein transforms human bone marrow mesenchymal cells into steroidogenic cells

Tomoko Tanaka[1], Shigeki Gondo[1], Taijiro Okabe[1], Kenji Ohe[1], Hisao Shirohzu[1], Hidetaka Morinaga[1], Masatoshi Nomura[1], Kenzaburo Tani[2], Ryoichi Takayanagi[1], Hajime Nawata[3] and Toshihiko Yanase[1]

[1]Department of Medicine and Bioregulatory Science, Graduate School of Medical Science, [2]Department of Molecular Genetics, Medical Institute of Bioregulation and [3]Graduate School of Medical Science, Kyushu University, Maidashi 3-1-1, Higashi-ku, Fukuoka 812-8582, Japan

(Correspondence should be addressed to T Yanase; Email: yanase@intmed3.med.kyushu-u.ac.jp)

Abstract

Steroidogenic factor 1/adrenal 4 binding protein (SF-1/Ad4BP) is an essential nuclear receptor for steroidogenesis as well as for adrenal and gonadal gland development. Mesenchymal bone marrow cells (BMCs) contain pluripotent progenitor cells, which differentiate into multiple lineages. In a previous study, we reported that adenovirus-mediated forced expression of SF-1 could transform mouse primary long-term cultured BMCs into steroidogenic cells. For future clinical application, trials using human BMCs would be indispensable. In this study, we examined whether SF-1 could transform human BMCs into steroidogenic cells and compared the steroid profile of these cellswith that of mouse steroidogenic BMCs. Primary cultured human BMCs infected with adenovirus containing bovine SF-1 cDNA could produce progesterone, corticosterone, cortisol, dehydroepiandrosterone, testosterone, and estradiol. Such a mixed character of adrenal and gonadal steroid production in human BMCs was supported by the expressions of P450scc, 3β-hydroxysteroid dehydrogenase (3β-HSD), P450c21, P450c11, P450c17, 17β-HSD, and P450arom mRNAs. Unlike mouse steroidogenic BMCs, introduction of SF-1 into human BMCs caused dramatic inductions of both ACTH and LH receptors, thus leading to good responsiveness of the cells to ACTH and LH respectively. Importantly, among several factors that are known to be closely associated with adrenal and/or gonadal development, introduction of only SF-1 enabled the human BMCs to express P450scc and to produce cortisol and testosterone, suggesting that SF-1 is truly a master regulator for the production of steroidogenic cells from human BMCs.

Journal of Molecular Endocrinology (2007) **39**, 343–350

Introduction

Steroidogenic factor 1 (SF-1) was initially identified as a ubiquitous transcription factor for steroidogenic genes (Yanase *et al.* 1991, Honda *et al.* 1993, Omura & Morohashi 1995, Parker & Schimmer 1997). SF-1 binds as a monomer to its responsive element located in the promoter regions of steroidogenic genes and enhances their transcriptional levels (Honda *et al.* 1993, Omura & Morohashi 1995, Parker & Schimmer 1997). In addition, the cAMP-protein kinase A signal pathway can strongly potentiate SF-1 transactivation activity (Fan *et al.* 2004). Since knockout mice for SF-1 show agenesis of both the adrenal glands and the gonads, as well as decreased expression levels of luteinizing hormone (LH) and follicle-stimulating hormone (FSH) in the pituitary gonadotroph (Ingraham *et al.* 1994, Luo *et al.* 1994, Morohashi & Omura 1996), SF-1 has been considered to be an essential factor for differentiation of the pituitary–adrenal or pituitary–gonadal axis. Dosage-sensitive sex reversal, adrenal hypoplasia congenital, critical region on the X chromosome gene 1 (DAX-1) is also an important factor for the development of this axis since patients with DAX-1 mutations show X-linked adrenal hypoplasia congenital (AHC) and hypogonadotropic hypogonadism (Muscatelli *et al.* 1994, Yanase *et al.* 1996). Thus, DAX-1 is considered to be involved in the differentiation process of the fetal adrenal gland. A tumor suppressor gene, Wilms' tumor 1 (WT1), was also proven to be related to urogenital development, including the development of the adrenal gland, from the findings of phenotypes in patients with mutations (Little & Wells 1997) and knockout mice (Wagner *et al.* 2003). Although their exact roles in humans are unknown, many other factors, such as pre-B-cell leukemia homeobox 1 (PBX-1; Schnabel *et al.* 2003), CBP/p300-interacting transactivator with Glu/Asp-rich C-terminal domain 2 (CITED2; Bamforth *et al.* 2001), wingless type MMTV integration site family member 4 (WNT4; Vainio *et al.* 1999), M33 (Katoh-Fukui *et al.* 1998), fibroblast growth factor 9 (Colvin *et al.* 2001), and GATA binding protein 4 (Tevosian *et al.* 2002), are also known to be involved in

0952–5041/07/039–343

DOI: 10.1677/JME-07-0076
Online version via http://www.endocrinology-journals.org

adrenal or gonadal development since disruption or overexpression of these genes in mice causes sex reversal or delayed sexual differentiation (Katoh-Fukui *et al.* 1998, Vainio *et al.* 1999, Bamforth *et al.* 2001, Colvin *et al.* 2001, Schnabel *et al.* 2003, Hammer *et al.* 2005).

In animal experiments, adrenocortical tissue has been successfully regenerated through xenotransplantation of cloned adrenocortical cells (Thomas *et al.* 1997), suggesting that the intraadrenal stem cells required for such tissue formation may be present in the adrenal cortex. Stable expression of SF-1 has been shown to direct embryonic stem cells toward the steroidogenic lineage. However, this steroidogenic capacity was very limited since progesterone was the only steroid produced in the presence of an exogenous substrate, 20α-hydroxycholesterol (Crawford *et al.* 1997).

Bone marrow cells (BMCs) may contribute to the regeneration of hematopoietic or mesenchymal lineages in multiple organs (Pittenger *et al.* 1999, Song & Tuan 2004). Therefore, we tested whether the introduction of SF-1 into mouse BMCs could produce steroidogenic cells (Gondo *et al.* 2004). We expanded a relatively pure BMC population by culturing the cells for 120–180 days, and then demonstrated that adenovirus-mediated forced expression of SF-1 in long-term cultured BMCs can produce steroidogenic cells with the capacity for *de novo* synthesis of various steroid hormones in response to adrenocorticotropic hormone (ACTH). Similar to our data, a recent report demonstrated that cAMP stimulation of a cloned mouse BMC line, KUM9, and human BMC line, hMSC-hTERT-E6/E7, stably expressing SF-1 induced cell differentiation into cells with a testis- and adrenal-type steroidogenic capacity respectively (Yazawa *et al.* 2006). These results suggest a promising utility of BMCs as a regenerative source of steroidogenic cells.

For the future clinical application of SF-1 in autologous cell transplantation therapy for patients with steroid hormone deficiency, it is very important to examine its effect on human BMCs. In this regard, we applied this technique to human BMCs and compared their steroidogenic profiles with those of mouse BMCs. In addition, we investigated the impacts of several known factors, WT1, DAX-1, PBX-1, CITED2, and WNT4, which are involved in adrenal and/or gonadal development, to determine whether the single introduction of each factor may also be sufficient to transform human BMCs into steroidogenic cells.

Materials and methods

Construction of the adenovirus and the lentivirus vectors

A recombinant adenovirus vector derived from the human type 5 adenovirus using a commercially available Adenovirus Expression Vector Kit (TakaraBio Ltd, Shiga, Japan), containing bovine SF-1 cDNA (Adx-bSF-1) or LacZ cDNA (Adx-LacZ) as a control, and was prepared as previously described (Gondo *et al.* 2004). Full-length human cDNAs for SF-1, WT1, DAX-1, PBX-1, CITED2, and WNT4 were cloned by reverse transcriptase-polymerase chain reaction (RT-PCR) using appropriate tissue total RNA with primers based on the GenBank database, subcloned into pCR-Blunt II-TOPO vector (Invitrogen) and then the entire sequences of these constructs were verified by sequencing. Each human cDNA was inserted into lentiviral vector (CS-CDF-CG-PRE, RIKEN BioResource Center, Tsukuba, Japan) and the preparation of each recombinant lentivirus was performed according to the manufacturer's protocol.

Culture of human mesenchymal BMCs and treatment with adenovirus or lentivirus

Human bone marrow mononuclear cells purchased from Cambrex (East Rutherford, NJ, USA) were cultured in nonhematopoietic (NH) Expansion medium (Miltenyi Biotec, Bergisch Gladbach, Germany) at 37 °C in a 5% CO_2 incubator for 4 weeks. Only adherent cells were used in the experiments. To test the capability for osteoblastic differentiation, $4{\cdot}5\times10^4$ cells were plated on 35 mm dish, cultured in NH OsteoDiff medium (Miltenyi Biotec) for 10 days and stained with alkaline phosphatase (Gondo *et al.* 2004). Adipogenic differentiation was confirmed at a cell density of $7{\cdot}5\times10^4$ cells/35 mm dish following treatment with NH AdipoDiff medium (Miltenyi Biotec) for 21 days and stained with Oil red O to test the capacity of cells to differentiate into mature adipocytes (Song & Tuan 2004).

Human BMCs (10^4 cells/well) were cultured on a collagen type I-coated 24-well plate, incubated in Adx-bSF-1 or Adx-LacZ medium at 37 °C for 1 h, rinsed with PBS, and cultured for 7 days. Culture medium was then changed and BMCs were cultured for another 4 days for measurements of steroid contents. In addition, human BMCs (10^4 cells/well) were cultured on a 24-well plate, incubated in NH Expansion medium containing lentivirus vector at 37 °C overnight, rinsed with PBS, and then cultured for another 10 days before being subjected to experiments.

Measurements of the steroid content in the medium secreted from human BMCs

Basal secretion levels of progesterone (P4), corticosterone (B), cortisol (F), aldosterone, testosterone (T), and estradiol (E_2) secreted into the culture medium were measured using an EIA kit (Cayman Chemical, Ann

Arbor, MI, USA). Dehydroepiandrosterone (DHEA) was measured using another EIA kit (Assay Designs, Ann Arbor, MI, USA). The detection limits of P4, B, F, aldosterone, T, E_2, and DHEA were 10, 38, 17, 21, 6, 8, and 15 pg/ml respectively. The secretions of F and T into the medium were also confirmed in the presence or absence of synthetic 1–24 ACTH (Shionogi Co., Osaka, Japan) or human chorionic gonadotropin (hCG; Aska Co. Ltd, Tokyo, Japan). Human BMCs were infected with Adx-bSF-1 (multiplicity of infection, MOI=20) and cultured for 7 days. Culture medium was then collected at day 11, and the cells were stimulated with 2·4 μM ACTH or 10 mU/ml hCG. Every 3–4 days, culture medium was collected for measurement of F and T concentrations and cells were treated with ACTH or hCG.

Quantitative real-time PCR

We performed quantitative analysis of the mRNA expression levels of ACTH receptor (ACTH-R), LH receptor (LH-R), and various steroidogenic enzymes including P450scc, 3β-hydroxysteroid dehydrogenase (3β-HSD), P450c21, P450c11, P450c17, P450ald, 17β-HSD type 3, and P450arom, by real-time PCR using a LightCycler (Roche Diagnostics GmbH) as described previously (Gondo *et al.* 2004). We isolated total RNA from cultured human BMCs using an RNeasy Mini kit (Qiagen, GmbH). We synthesized first-strand complimentary DNA using 1 μg total RNA as a template with QuantiTect RT kit (Qiagen) and carried out PCR in a LightCycler according to the manufacturer's instructions. We used the carefully designed sense/antisense primers of P450scc, 3β-HSD, P450c21, P450c11, P450ald, 17β-HSD type 3, ACTH-R, LH-R, P450arom, and β-actin (TakaraBio). PCR primers and conditions are available on request. Threshold values were obtained where fluorescent intensity was in the geometric phase of amplification, as determined with LightCycler Software Ver. 3.5. Products were verified on 2% agarose gels. We verified the nucleotide sequences of each PCR product by direct sequencing using the appropriate primers. Relative expression levels of the mRNAs were calibrated to those of β-actin.

Flowcytometry

The protocol essentially followed a previously described method (Hirase *et al.* 2000). Briefly, 1×10^5 BMCs were incubated with either phycoerythin (PE)-conjugated anti-human c-kit, CD11b, CD31, CD34, CD44, CD45, and CD105 monoclonal antibodies (BD Biosciences, Franklin Lakes, NJ, USA) or an isotype-matched PE-conjugated mouse IgG (BD Biosciences) for 30 min at 4 °C. The cells were finally analyzed on a FACScan flowcytometer (BD Biosciences).

Immunofluorescence cell staining

We conducted immunofluorescence cell staining of BMCs using goat anti-ACTH-R and anti-LH-R antibodies (Santa Cruz Biotechnology Inc., Santa Cruz, CA, USA), rabbit antibody against bovine SF-1 (kindly provided by Prof. Morohashi, Kyushu University, Japan), Alexa Fluor 488 donkey anti-rabbit IgG and Alexa Fluor 594 rabbit anti-goat IgG (Molecular Probes, Eugene, OR, USA). Inoculated cells were plated onto CC2-treated chamber slides (Nalge Nunc International Co., Naperville, IL, USA), cultured for 3 days and fixed with 4% paraformaldehyde at 4 °C for 1 h. Immunofluorescence cell staining was then performed according to the manufacturer's protocol. The fluorescence was observed using fluorescence microscopy Biozero (Keyence, Tokyo, Japan).

Immunoblotting

Human BMCs were washed with PBS and lysed in CelLytic M cell lysis reagent (Sigma). A total of 20 μg protein was subjected to SDS-PAGE and transferred onto a PVDF membrane (Bio-Rad Laboratories). Western blotting was performed according to the manufacturer's protocol. Protein levels were visualized using an ECL Plus kit (GE Healthcare, Buckinghamshire, UK) and a LAS3000 detector (Fuji Film, Tokyo, Japan).

Statistical analysis

One-factor ANOVA was used for statistical evaluation. $P<0·05$ was considered to be statistically significant.

Results

Flowcytometric analyses revealed that the human BMCs prepared for steroidogenic transformation were negative for the surface markers including CD45 (leukocyte marker), CD11b (monocyte/macrophage marker), CD34, c-kit (hematopoietic stem cell markers), and CD31 (endothelial cell marker) but positive for CD44 and CD105 (potential marker for mouse mesenchymal cells; data not shown). Although the BMCs in our experiment still constitute a heterogeneous population, the analysis of cell surface markers strongly suggested the possibility that the steroid-producing cells originate from multipotent and immature stem cells. Importantly, human BMCs differentiated into an osteoblastic phenotype and adipocyte phenotype following respective proper treatment (data not shown), suggesting that the character of the human BMCs may be much closer to that of mesenchymal BMC lineages. These results suggest that

steroid-producing cells originate from multipotent and immature stem cells.

The above human mesenchymal BMCs were inoculated with Adx-bSF-1 (MOI=0, 10, 50, 100, and 200) and cultured for 3, 7, and 11 days. We analyzed the expression level of SF-1 using antibody against SF-1. The bovine SF-1 expression was observed predominantly in the nucleus of most of the cultured human BMCs even by minimal infection at MOI of 10 (Fig. 1A). The expression level seems to be increased in a MOI-dependent manner as shown by immunofluorescence staining at day 3 (Fig. 1A) and by western blot analysis at day 11 (Fig. 1B). Thus, the following experiments were performed 10 days after infection. As in mouse cells (Gondo *et al.* 2004), throughout these experiments, induction of endogenous SF-1, namely the expression of human SF-1 was not observed by real-time PCR (data not shown).

First, to quantify the basal secretion levels of steroid hormones, cultured medium (day 11) of human BMCs infected with Adx-bSF-1 or Adx-LacZ was analyzed. Cells were infected with Adx-bSF-1 and cultured for 7 days. The steroid content accumulating in the medium over the next 4 days was then measured. Progesterone (P4) secretion was increased with a dependency on MOI of Adx-bSF-1, namely SF-1 expression level (data not shown). The secretions of P4, corticosterone (B), cortisol (F), aldosterone, DHEA, testosterone (T), and E_2 into the medium from human BMCs infected with Adx-bSF-1 (MOI=50) were increased when compared with non-infected cells (MOI=0) or cells infected with Adx-LacZ (MOI=50; Fig. 2A). To investigate whether steroid synthetic enzymes were upregulated in human BMCs infected with Adx-bSF-1, the mRNA levels of such enzymes were analyzed by real-time PCR (Fig. 2B). The expression levels of P450scc, 3β-HSD, P450c21, P450c11, P450c17, 17β-HSD type 3, and P450arom mRNAs relative to β-actin, expressed as the ratio to those of non-infected BMCs (MOI=0), were significantly increased with increasing SF-1 expression level; cells infected with Adx-LacZ did not show such a phenomenon (Fig. 2B). Despite the presence of aldosterone production, we could not detect P450ald by real-time PCR.

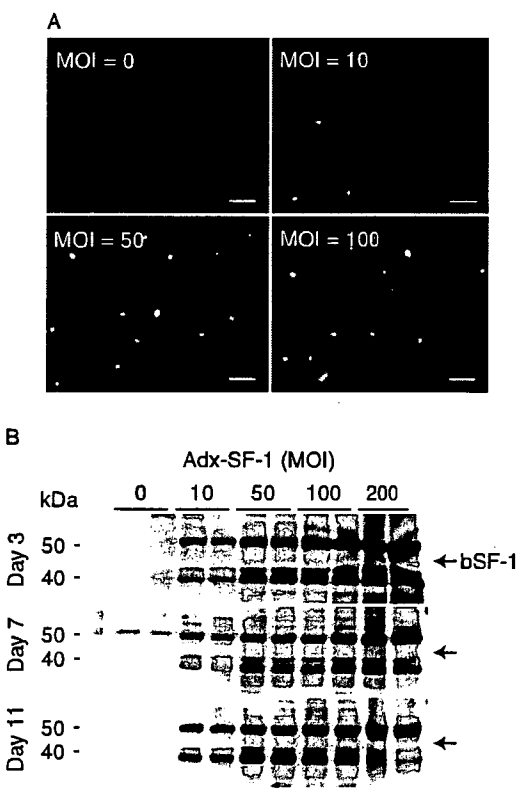

Figure 1 SF-1 expression in human BMCs infected with adenovirus vector. Human BMCs were inoculated with Adx-bSF-1 (MOI=0, 10, 50, 100, or 200) and cultured for 3, 7, and 11 days. To analyze the expression level of bSF-1, infected cells were subjected to (A) immunofluorescence staining and total cell lysate was subjected to (B) immunoblot analysis using an antibody against SF-1 (please see Materials and methods). The bar indicates a 100 μm scale.

In Adx-bSF-1-infected human BMCs, the mRNA expression levels of both ACTH-R and LH-R relative to β-actin were increased in a MOI-dependent manner (Fig. 3A), while those in cells infected with Adx-LacZ was undetectable. Next, human BMCs were infected with Adx-bSF-1 or Adx-LacZ (MOI=200), and 3 days later they were stained with specific antibodies against the ACTH-R, LH-R, or SF-1. As a result, both receptors were detected in SF-1-positive cells, suggesting actual inductions of both receptors by SF-1 (Fig. 3B). At 3 day intervals after infection of the cells with Adx-bSF-1 (MOI=20), the cells were stimulated with 2·4 μM ACTH or 10 mU/ml hCG. After stimulation the medium was collected for the measurement of steroid content. The secretion of cortisol into the medium was increased in response to both 2·4 μM ACTH and 10 mU/ml hCG stimulation (Fig. 3C). The maximum response of cortisol to ACTH or hCG was observed on day 21, when cortisol production was increased by 9·5- and 6-fold in response to ACTH and hCG respectively. Likewise, the secretion of testosterone was increased in response to both hCG and ACTH stimulation, and the maximum response was obtained at day 18 (Fig. 3C). Together, these data indicate a capability of human mesenchymal BMCs to be transformed into steroidogenic cells, which are capable of responding to ACTH and LH.

Finally, we tested the effects of several factors that are reported to be associated with adrenal and/or gonadal development, mainly based on the results of human or mouse phenotypes due to a complete or partial lack of each factor (Muscatelli *et al.* 1994, Yanase *et al.* 1996, Vainio *et al.* 1999, Bamforth *et al.* 2001, Schnabel *et al.*

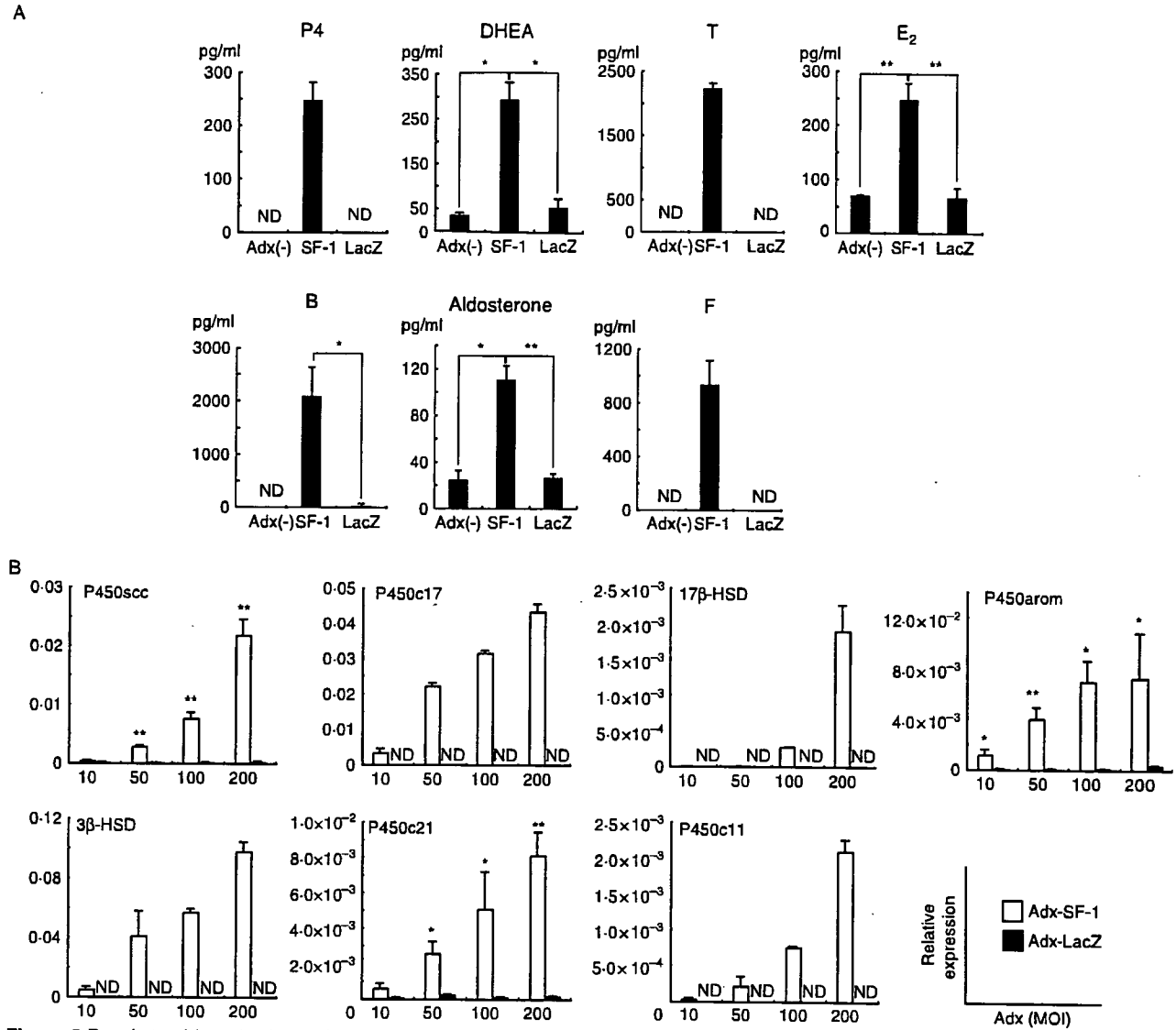

Figure 2 Basal steroid production and mRNA expression levels of steroidogenic enzymes in human BMCs infected with Adx-bSF-1. Cells were infected with Adx-bSF-1 and cultured for 7 days. The steroid content accumulated in the medium over the next 4 days was then measured. (A) Basal secretion of progesterone (P4), corticosterone (B), aldosterone, cortisol (F), DHEA, testosterone (T), and estradiol (E_2) into the medium from the human BMCs infected with Adx-bSF-1 (MOI=0, 50) or Adx-LacZ (MOI=50). (B) Real-time PCR analysis of the expression levels of P450scc, 3β-HSD, P450c11, P450c21, P450c17, 17β-HSD type 3, and P450arom mRNAs in human BMC cells infected with Adx-bSF-1 or Adx-LacZ. The mRNA expression levels relative to the levels of β-actin are expressed. Values represent the means±S.D. ($n=3$). $^*P<0.05$, $^{**}P<0.01$.

2003). The tested factors were SF-1 as a positive control, GFP as a negative control, WT1, DAX-1, PBX-1, CITED2, and WNT4. WT1 encodes a zinc finger transcription factor. Alternative splicing of exon 5 results in a 17 amino acid insertion, and alternative splicing of exon 9 produces an insertion three amino acid Lys-Thr-Ser (KTS). Alternative splicing these two sites gives rise to four different protein isoforms designated A, B, C, and D; or (−/−), (+/−), (−/+), and (+/+), representing the presence or absence of exon 5 and KTS respectively (Haber *et al.* 1991). In this experiment, for more convenience in the preparation or infection of cells with vector, cells were infected with lentivirus containing each factor. In a preliminary experiment, the expression of each factor was confirmed by real-time PCR or western blotting of the respective infected cells, 10 days after infection (data not shown). Therefore, 10 days after infection, the medium was changed and the F and T content in the medium on each of the next 4 days (day 11–14 days) were measured; the expression levels of P450scc in cells at day 14 were also determined by real-time PCR. Introduction

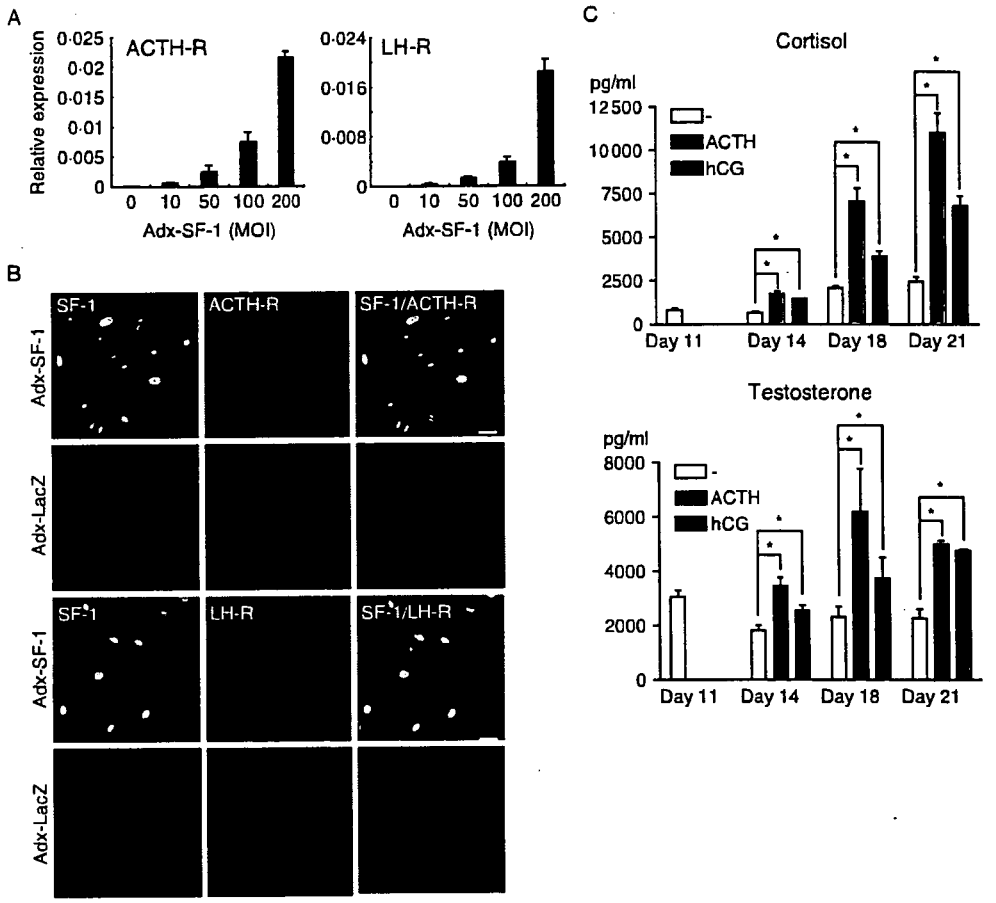

Figure 3 Expression of ACTH-R and LH-R and responsiveness to ATCH and LH in cultured human BMCs. (A) Human BMCs infected with Adx-bSF-1 or Adx-LacZ were cultured for 11 days and then the expression levels of ACTH-R and LH-R were determined by real-time PCR. (B) Human BMCs infected with Adx-bSF-1 or Adx-LacZ (MOI = 200) were cultured for 3 days, and then the expression levels of ACTH-R and LH-R were determined by immunofluorescence staining using antibodies against SF-1 and ACTH-R or LH-R The bar indicates a 50 μm scale. (C) The effect of ACTH and LH on the secretion of cortisol and testosterone respectively, from cultured human BMCs. Human BMCs were infected with Adx-bSF-1 (MOI = 20) and cultured for 7 days. Culture medium was then collected at day 11 for measurement of basal secretions of steroids, and the cells were stimulated with 2·4 μM ACTH or 10 mU/ml hCG. Every 3–4 days, culture medium was collected for measurement of cortisol and testosterone concentrations and cells were treated with ACTH or hCG. The secretion of cortisol or testosterone into the medium was increased in response to ACTH and hCG stimulation respectively. Values represent the means ± S.D. ($n = 3$). $P < 0·05$ against the control (absence of ACTH or hCG).

of SF-1 only into human BMCs induced a 4·7-fold induction of P450scc expression when compared with GFP, and caused 11·3- and 12·5-fold increase in the secretion of F and T into the medium respectively. Single introductions of WT1 (−/−, −/+, +/−, and +/+), DAX-1, PBX-1, CITED2, and WNT4 did not produce any such effects (data not shown).

Discussion

Although the character of human mesenchymal stem cells has not been fully clarified and remains controversial, steroid-producing cells may originate from multipotent and immature stem cells. Importantly, human cultured BMCs were able to differentiate into an osteoblastic or adipocyte phenotype following appropriate treatments, suggesting that the character of the prepared human BMCs may be much closer to mesenchymal BMC lineages. Under such conditions, we demonstrated, for the first time, that human BMCs infected with Adx-bSF-1 can produce significant amounts of progesterone, corticosterone, cortisol, DHEA, testosterone, and estradiol, owing to the expression of mRNAs for P450scc, 3β-HSD, P450c11, P450c21 P450c17, 17β-HSD type 3, and P450arom, as detected by RT-PCR. Most of the profiles of steroidogenic enzymes were quite similar to those in mouse

BMCs (Gondo *et al.* 2004), except for the finding that P450c21 is expressed in human cells but not in mouse cells. Although we observed a significant amount of aldosterone production, we could not show the expression of P450ald by real-time PCR (data not shown). Thus, we cannot completely conclude a capability of human BMCs for aldosterone production. Further studies are needed on this point including the optimization of PCR conditions. As in mouse cells (Gondo *et al.* 2004), the steroid profile of cultured human BMCs showed a mixed pattern of adrenal and gonadal steroidogenesis, namely the simultaneous production of cortisol and sex steroids. This finding matches well an established concept that common precursor cells divide into two distinct characteristic cell types, designated adrenal precursor cells and bipotential gonadal precursor cells, and finally develop into the adrenal cortex or testes and ovaries, respectively, under the regulation of many transcriptional factors, including SF-1 (Yanase *et al.* 2006).

A feature of human steroidogenic cells that makes them remarkably distinct from mouse cells is the clear induction of ACTH-R and LH-R following the introduction of SF-1. Mouse BMCs originally expressed ACTH-R without introduction of SF-1, namely predominant expression of an adipose tissue type of ACTH-R (Kubo *et al.* 2004), rather than an adrenal tissue type of ACTH-R (Cammas *et al.* 1997). The introduction of SF-1 itself did not increase ACTH-R expression in mouse BMCs, since the promoter region of the adipose tissue type ACTH-R gene does not contain SF-1 sites, unlike the promoter of the adrenal type ACTH-R gene (Cammas *et al.* 1997). On the other hand, the gene encoding the human ACTH receptor does not seem to produce extra-adrenal type isoform from its gene structure (Kubo *et al.* 2004) and produces only adrenal type receptor, which can be responsive to SF-1; mRNA for this receptor was expressed in human BMCs (data not shown). Similarly, LH-R was dramatically induced in human BMCs, but not in mouse BMCs. The human LH-R gene promoter also contains a potential SF-1 site, although binding SF-1 to this site is not proven (Geng *et al.* 1999). There may be an unknown SF-1 induced factor that promotes the expression of LH-R. Anyway, the findings of good induction of ACTH-R and LH-R in human BMCs and responsiveness of these cells to ACTH and LH are physiologically important when we consider a future clinical application for autologous BMC transplantation into patients with steroid insufficiency.

In humans, sex-determining region Y (SRY) initiates the testis-determining pathway by inducing the expression of a series of downstream factors, including SF-1, WT1, DAX-1, SRY-related genes HMG-box 9, and several other factors, thus resulting in a male phenotype (Yanase *et al.* 2006). In this pathway, SF-1 has been considered to be a master regulator that controls the overall stream of the developmental mechanism. WT1 seems to be of interest because, in contrast to the adrenal agenesis seen in mice lacking all Wt1 transcript (Wagner *et al.* 2003), analyses of mice with isoform-specific disruption of Wt1 have shown different roles for two alternatively spliced transcripts the −KTS and +KTS isoforms (Hammes *et al.* 2001). Namely, selective inactivation of the +KTS isoform did not impair ovary development, but rather impaired testis and male sex differentiations. PBX-1 is a homeodomain protein that contributes to adrenal development since, PBX-1 KO mice, which die *in utero* due to defects in multiple organs, completely lacked adrenal glands and had impaired testis development associated with decreased proliferation in the urogenital ridges (Schnabel *et al.* 2003). A coactivator CITED2 coregulates genes that are essential for adrenal development since its KO mice were found to have adrenal agenesis (Bamforth *et al.* 2001). Wnt proteins act via the frizzled receptor family to initiate a canonical cascade of intracellular signals leading to β-catenin accumulation in the nucleus and subsequent transactivation of downstream target genes (Tolwinski & Wieschaus 2004). Disruption of WNT4 in mice causes a marked masculinization of XX females with absence of the female Mullerian duct and persistence of the male Wolffian duct derivatives due to excess gonadal testosterone synthesis, and abnormal differentiation of the definitive zone in the adrenal gland (Vainio *et al.* 1999).

While, admittedly, the present experiment was preliminary in that we have not dealt with all known factors, we tested whether the above factors, which are closely associated with sexual differentiation including adrenal and/or gonadal development, could transform human BMCs into steroidogenic cells. Our finding that only SF-1 among SF-1, WT1, DAX-1, PBX-1, CITED2, and WNT4 could transform human BMCs into steroidogenic cells suggested that SF-1 is truly a master regulator, even for the production of steroidogenic cells from human mesenchymal BMCs. However, it is also important to test the functional relationship between SF-1 and other factors involved in steroidogenesis by multiple transfections, because sexual differentiation takes place in a series of cascades of various factors (Yanase *et al.* 2006). Such detailed experiments are currently underway in our laboratory.

In summary, we showed that SF-1 could transform human bone marrow mesenchymal cells into steroidogenic cells. This finding is expected to develop extensively in the near future, possibly leading to the development of therapies to relieve the many patients who are forced to take hormone replacement therapy.

Acknowledgements

We acknowledge the support of Health and Labour Sciences Research Grant and grant of Ministry of Education, Culture, Sports, Science and Culture (No. 16086207: Molecular mechanisms of sex differentiation). The authors declare that there is no conflict of interest that would prejudice the impartiality of this scientific work.

References

Bamforth SD, Braganca J, Eloranta JJ, Murdoch JN, Marques FI, Kranc KR, Farza H, Henderson DJ, Hurst HC & Bhattacharya S 2001 Cardiac malformations, adrenal agenesis, neural crest defects and exencephaly in mice lacking Cited2, a new Tfap2 co-activator. *Nature Genetics* **29** 469–474.

Cammas FM, Pullinger GD, Barker S & Clark AJ 1997 The mouse adrenocorticotropin receptor gene: cloning and characterization of its promoter and evidence for a role for the orphan nuclear receptor steroidogenic factor 1. *Molecular Endocrinology* **11** 867–876.

Colvin JS, Green RP, Schmahl J, Capel B & Ornitz DM 2001 Male-to-female sex reversal in mice lacking fibroblast growth factor 9. *Cell* **104** 875–889.

Crawford PA, Sadovsky Y & Milbrandt J 1997 Nuclear receptor steroidogenic factor 1 directs embryonic stem cells toward the steroidogenic lineage. *Molecular and Cellular Biology* **17** 3997–4006.

Fan W, Yanase T, Wu Y, Kawate H, Saitoh M, Oba K, Nomura M, Okabe T, Goto K, Yanagisawa J *et al.* 2004 Protein kinase A potentiates adrenal 4 binding protein/steroidogenic factor 1 transactivation by reintegrating the subcellular dynamic interactions of the nuclear receptor with its cofactors, general control nonderepressed-5/transformation/transcription domain-associated protein, and suppressor, dosage-sensitive sex reversal-1: a laser confocal imaging study in living KGN cells. *Molecular Endocrinology* **18** 127–141.

Geng Y, Tsai-Morris CH, Zhang Y & Dufau ML 1999 The human luteinizing hormone receptor gene promoter: activation by Sp1 and Sp3 and inhibitory regulation. *Biochemical and Biophysical Research Communications* **263** 366–371.

Gondo S, Yanase T, Okabe T, Tanaka T, Morinaga H, Nomura M, Goto K & Nawata H 2004 SF-1/Ad4BP transforms primary long-term cultured bone marrow cells into ACTH-responsive steroidogenic cells. *Genes to Cells* **9** 1239–1247.

Haber DA, Sohn RL, Buckler AJ, Pelletier J, Call KM & Housman DE 1991 Alternative splicing and genomic structure of the Wilms tumor gene WT1. *PNAS* **88** 9618–9622.

Hammer GD, Parker KL & Schimmer BP 2005 Minireview: transcriptional regulation of adrenocortical development. *Endocrinology* **146** 1018–1024.

Hammes A, Guo JK, Lutsch G, Leheste JR, Landrock D, Ziegler U, Gubler MC & Schedl A 2001 Two splice variants of the Wilms' tumor 1 gene have distinct functions during sex determination and nephron formation. *Cell* **106** 319–329.

Hirase N, Yanase T, Mu Y, Muta K, Umemura T, Takayanagi R & Nawata H 2000 Thiazolidinedione suppresses the expression of erythroid phenotype in erythroleukemia cell line K562. *Leukemia Research* **24** 393–400.

Honda S, Morohashi K, Nomura M, Takeya H, Kitajima M & Omura T 1993 Ad4BP regulating steroidogenic P-450 gene is a member of steroid hormone receptor superfamily. *Journal of Biological Chemistry* **268** 7494–7502.

Ingraham HA, Lala DS, Ikeda Y, Luo X, Shen WH, Nachtigal MW, Abbud R, Nilson JH & Parker KL 1994 The nuclear receptor steroidogenic factor 1 acts at multiple levels of the reproductive axis. *Genes and Development* **8** 2302–2312.

Katoh-Fukui Y, Tsuchiya R, Shiroishi T, Nakahara Y, Hashimoto N, Noguchi K & Higashinakagawa T 1998 Male-to-female sex reversal in M33 mutant mice. *Nature* **393** 688–692.

Kubo M, Shimizu C, Kijima H, Nagai S & Koike T 2004 Alternate promoter and 5′-untranslated exon usage of the mouse adrenocorticotropin receptor gene in adipose tissue. *Endocrine Journal* **51** 25–30.

Little M & Wells C 1997 A clinical overview of WT1 gene mutations. *Human Mutation* **9** 209–225.

Luo X, Ikeda Y & Parker KL 1994 A cell-specific nuclear receptor is essential for adrenal and gonadal development and sexual differentiation. *Cell* **77** 481–490.

Morohashi KI & Omura T 1996 Ad4BP/SF-1, a transcription factor essential for the transcription of steroidogenic cytochrome P450 genes and for the establishment of the reproductive function. *FASEB Journal* **10** 1569–1577.

Muscatelli F, Strom TM, Walker AP, Zanaria E, Recan D, Meindl A, Bardoni B, Guioli S, Zehetner G, Rabl W *et al.* 1994 Mutations in the DAX-1 gene give rise to both X-linked adrenal hypoplasia congenita and hypogonadotropic hypogonadism. *Nature* **372** 672–676.

Omura T & Morohashi K 1995 Gene regulation of steroidogenesis. *Journal of Steroid Biochemistry and Molecular Biology* **53** 19–25.

Parker KL & Schimmer BP 1997 Steroidogenic factor 1: a key determinant of endocrine development and function. *Endocrine Reviews* **18** 361–377.

Pittenger MF, Mackay AM, Beck SC, Jaiswal RK, Douglas R, Mosca JD, Moorman MA, Simonetti DW, Craig S & Marshak DR 1999 Multilineage potential of adult human mesenchymal stem cells. *Science* **284** 143–147.

Schnabel CA, Selleri L & Cleary ML 2003 Pbx1 is essential for adrenal development and urogenital differentiation. *Genesis* **37** 123–130.

Song L & Tuan RS 2004 Transdifferentiation potential of human mesenchymal stem cells derived from bone marrow. *FASEB Journal* **18** 980–982.

Tevosian SG, Albrecht KH, Crispino JD, Fujiwara Y, Eicher EM & Orkin SH 2002 Gonadal differentiation, sex determination and normal Sry expression in mice require direct interaction between transcription partners GATA4 and FOG2. *Development* **129** 4627–4634.

Thomas M, Northrup SR & Hornsby PJ 1997 Adrenocortical tissue formed by transplantation of normal clones of bovine adrenocortical cells in scid mice replaces the essential functions of the animals' adrenal glands. *Nature Medicine* **3** 978–983.

Tolwinski NS & Wieschaus E 2004 Rethinking WNT signaling. *Trends in Genetics* **20** 177–181.

Vainio S, Heikkila M, Kispert A, Chin N & McMahon AP 1999 Female development in mammals is regulated by Wnt-4 signalling. *Nature* **397** 405–409.

Wagner KD, Wagner N & Schedl A 2003 The complex life of WT1. *Journal of Cell Science* **116** 1653–1658.

Yanase T, Simpson ER & Waterman MR 1991 17 alpha-hydroxylase/17,20-lyase deficiency: from clinical investigation to molecular definition. *Endocrine Reviews* **12** 91–108.

Yanase T, Takayanagi R, Oba K, Nishi Y, Ohe K & Nawata H 1996 New mutations of DAX-1 genes in two Japanese patients with X-linked congenital adrenal hypoplasia and hypogonadotropic hypogonadism. *Journal of Clinical Endocrinology and Metabolism* **81** 530–535.

Yanase T, Gondo S, Okabe T, Tanaka T, Shirohzu H, Fan W, Oba K, Morinaga H, Nomura M, Ohe K *et al.* 2006 Differentiation and regeneration of adrenal tissues: an initial step toward regeneration therapy for steroid insufficiency. *Endocrine Journal* **53** 449–459.

Yazawa T, Mizutani T, Yamada K, Kawata H, Sekiguchi T, Yoshino M, Kajitani T, Shou Z, Umezawa A & Miyamoto K 2006 Differentiation of adult stem cells derived from bone marrow stroma into Leydig or adrenocortical cells. *Endocrinology* **147** 4104–4111.

Received in final form 10 September 2007
Accepted 15 September 2007
Made available online as an Accepted Preprint
20 September 2007

Available online at www.sciencedirect.com
ScienceDirect
Cancer Letters 260 (2008) 20–27
CANCER Letters
www.elsevier.com/locate/canlet

Inhibition of proteasome activity sensitizes human granulosa tumor cells to TRAIL-induced cell death

Dori C. Woods [a], Han-Ken Liu [a], Yoshihiro Nishi [b], Toshihiko Yanase [b], A.L. Johnson [a,*]

[a] *Department of Biological Sciences and the Walther Cancer Research Center, The University of Notre Dame, Notre Dame, IN 46556, USA*
[b] *Department of Medicine and Bioregulatory Science, Graduate School of Medical Sciences, Kyusyu University, Fukuoka 812-8582, Japan*

Received 27 August 2007; received in revised form 12 October 2007; accepted 15 October 2007

Abstract

Human granulosa tumor cell (GCT) lines (KGN and COV434) were utilized to establish the combinatorial effects of TRAIL treatment and a proteasome inhibitor on cell viability, *in vitro*. TRAIL induced a slight, but consistent, decrease in viability for both cell lines, and pharmacologic inhibition of proteasome activity, using Z-LLF-CHO (Z-LLF), synergistically enhanced TRAIL-induced loss of viability. This enhanced sensitization was associated with the up-regulation of a TRAIL receptor, DR5, and pro-apoptotic Bax. Targeted reduction of p53 expression revealed that the ability of Z-LLF to enhance DR5 and Bax expression occurs independent of p53 activity. These studies underscore the potential to develop targeted treatments for GCTs using established cell lines.

Keywords: Granulosa cell tumors; TRAIL; Proteasome; p53; Apoptosis

1. Introduction

Granulosa cell tumors (GCTs) represent less than 5% of all ovarian neoplasms, yet the etiology, genetics, and particularly pharmacologic management of GCTs have been understudied compared to ovarian surface epithelium (OSE)-derived cancers. Due to the paucity of published reports regarding targeted GCT therapy, the prevailing treatment is derived from cancers originating from human (h) OSE, despite the fact that granulosa cells demonstrate a unique phenotype [1,2]. Foremost among their defining characteristics is included the capacity for steroid production, placing GCTs within the category of an endocrine tumor. The lack of information regarding selective treatment for GCTs is due in large part to the scarcity of appropriate *in vitro* model systems, and in particular, transformed granulosa cell lines that express functional gonadotropin receptors. The recent description of the GCT lines, KGN [3], together with COV434 [4], has provided new opportunities for developing targeted GCT therapies.

Although considerable information exists regarding the efficacy of the naturally occurring

* Corresponding author. Tel.: +1 574 631 9450; fax: +1 574 631 7413.
E-mail address: Johnson.128@nd.edu (A.L. Johnson).

0304-3835/$ - see front matter © 2007 Elsevier Ireland Ltd. All rights reserved.
doi:10.1016/j.canlet.2007.10.016

cytokine, tumor necrosis factor-related apoptosis-inducing ligand (TRAIL), in a variety of cancers (including those of hOSE origin) [5], the efficacy of TRAIL to target GCTs has not been reported. Interest in the therapeutic use of TRAIL originates from studies demonstrating its cytotoxicity in tumor cells, while most normal cells are resistant to TRAIL-induced apoptosis [6]. Of note is that recent evidence from primary cultured ovarian granulosa cells indicates that healthy granulosa cells are normally resistant to TRAIL-induced apoptosis [7].

The apoptosis-inducing effects of TRAIL in cancerous cells are mediated through one or more death receptors (e.g., DR4 or DR5) belonging to the tumor necrosis factor receptor (TNFR) superfamily [8–10]. These death receptors are distinguished by the presence of multiple cysteine-rich domains within the extracellular domain, plus a well-characterized intracellular death domain (DD) [11,12]. Upon binding with TRAIL, the DD associates with Fas-associated death domain (FADD) protein, forming an apoptosis-inducing signaling complex (DISC) [11]. The death-effector domain (DED) of FADD subsequently interacts with the DED of the initiator caspase, caspase-8 [12]. Dimerization and activation of caspase-8 cleaves bid, the C-terminus of which triggers the release of mitochondrial cytochrome *c*. This series of events leads to formation of the apoptosome complex, followed by the downstream activation of caspase-9 and eventually caspase-3 [13,14].

There is accruing evidence from a variety of primary cells and cancer cell lines that inhibitors of proteasome activity induce apoptosis, mediated in part through the pro-apoptotic protein, Bax [15–18]. The activation of Bax is associated with release of mitochondrial cytochrome *c*, and downstream effector caspase activation [19]. Moreover, it has been reported that proteasome inhibitors mediate apoptosis in multiple cancer cell lines through enhanced p53 activity [20], and that the actions of p53 occur, in part, through increased transcription of *bax* and *dr5* [21–23]. It has recently been documented that primary cultured granulosa cells can be rendered sensitive to TRAIL when treated in combination with a proteasome inhibitor in the hen [8]. Nevertheless, the potential for sensitizing effects of proteasome inhibitors on TRAIL-induced apoptosis and its dependency on p53 expression specifically in GCTs has yet to be evaluated.

2. Materials and methods

2.1. Cell culture and reagents

The human GCT line, COV434, was generously provided by Dr. De Geyter (University of Basel, Switzerland), while establishment of the KGN line has been described [3]. COV434 cells were cultured in DMEM + 10% FBS (Invitrogen), while KGN cells were cultured in DMEM:F12 + 10% FBS. Both cell lines were maintained in a sub-confluent state during all experiments, and maintained at 37 °C in 5% CO_2/95% humidified air. For cell culture experiments, adherent cells were removed from culture flasks and plated in 6-, 12- or 96-well Corning polystyrene cell culture dishes. Recombinant human TRAIL was purchased from Peprotech (Rocky Hill, NJ), Z-LLF-CHO (Z-LLF) was from Calbiochem (San Diego, CA), while Z-IETD-FMK (IETD) and Z-LEHD-FMK (LEHD) were from R&D Systems (Minneapolis, MN). The effective doses for TRAIL, Z-LLF-CHO, Z-IETD-FMK and Z-LEHD-FMK were empirically determined for each cell line.

2.2. Cell viability assay

Cells were seeded in a 96-well cell culture plate at a density of 2×10^4 (COV434) or 1×10^4 (KGN) and treated with Z-LLF (2–20 μM), TRAIL (3–200 ng/ml), alone or in combination. Following the time period specified for each experiment, cytotoxic effects were evaluated by monitoring metabolic activity with a methyl tetrazolium salt (MTS) assay (a measure of cell viability) using the CellTiter 96 Aqueous One reagent (Promega, Madison, WI) [7].

2.3. Western blot analysis

Western blot analysis was completed as previously described [24]. The rabbit anti-DR5 serum was from Sigma (diluted 1:500). The rabbit anti-Bax serum and mouse monoclonal anti-p53 immunoglobulin were from Santa Cruz (Santa Cruz, CA; diluted 1:1000 and 1:100, respectively). The horseradish peroxidase-conjugated anti-rabbit and anti-mouse secondary antibodies were from Pierce (Rockford, IL; 1:10,000). Membranes were incubated with ECL Western blotting detection reagent (Pierce) for 1 min, wrapped and exposed to X-ray film for 3–10 min.

2.4. Real-time quantitative PCR

Forward and reverse primers for *dr5*, *bax*, *p53*, and *18 s* rRNA were generated using MacVector software (MacVector, Inc., Cary, NC), and validated for use with real-time PCR by determining the optimal amplification efficiency and primer concentrations as described by the manufacturer (Applied Biosystems, Foster City, CA). Pri-

mer sequences utilized were *dr5* forward (FW): 5′-*GAATG ACCTCCTTTTCTGCTTGC*-3′, *dr5* reverse (RV): 5′-*GC TTCCCCACTGTGCTTTGTA*-3′ (GenBank Accession No. AF020501); *bax* FW 5′-*TGCTGGCAAAGTAGAA AAGGGC*-3′, *bax* RV 5′-*TGCTGGCAAAGTAGA AAAGGGGC*-3′ (NM_138761); *p53* FW 5′-GCAGCTG TGGGTTGATTCCACA-3′, p53 RV: 5′-GCCTGGGC ATCCTTGAGTTC-3′ (NM_000546) [25]; 18 s FW: 5′-*A AACGGCTACCACATCCAAG*-3′, 18 s RV 5′-*CCTCC AATGGATCCTGGTTA*-3′ (NR_003286).

Random-primed, reverse transcribed cDNA synthesis reactions were performed using the Promega Reverse Transcription System (Promega). For real-time PCR, primers were added to 25 μl total reaction volume using reagents provided in the ABgene Absolute QPCR Sybr Green Mix (ABgene, Rochester, NY). Reactions were completed on the ABI 7700 Thermocycler (Applied Biosystems). Conditions were set to the following parameters: 15 min at 95 °C followed by 40 cycles each of 15 s at 95 °C, 30 s at 60 °C, 30 s at 72 °C. The C_t (defined as the cycle number at which the fluorescence exceeds a threshold level) was determined for each reaction (run in triplicate) using the Sequence Detection software (v.1.6.3), while quantification was accomplished using the $\Delta\Delta C_t$ method [26]. Values are expressed as fold-difference compared to an appropriate control sample.

2.5. Transfection with p53 siRNA

Transfections were performed using Lipofectamine 2000 transfection reagent, as described by the manufacturer (Invitrogen). Briefly, cells were plated overnight in medium containing 10% FBS, then medium was removed and cells were rinsed once with PBS. Cells were cultured in serum- and antibiotic-free medium containing Lipofectamine (mock), Lipofectamine plus non-coding (control) siRNA complex, or Lipofectamine plus siRNA for p53 (sip53) targeting duplexes (Santa Cruz). The cells were cultured with complexes for 5 h, followed by the addition of an equal amount of medium containing 20% FBS and an additional 24 h culture. Knock-down efficiency was evaluated by PCR and Western blot analysis.

2.6. Confocal microscopy

KGN cells were seeded onto cover slips and cultured for 24 h. Cells were subsequently treated with Z-LLF (10 μM) for an additional 8 h. MitoTracker (200 μM; Invitrogen) was added during the last 45 min for visualization of mitochondria. Cells were rinsed with phosphate-buffered saline (PBS) and fixed with 2% paraformaldehyde for 45 min, rinsed again and incubated in blocking buffer, and finally incubated with cytochrome *c* antibody (BD Biosciences, San Jose, CA; diluted 1:100) for 2 h at room temperature. Cells were washed prior to incubation with fluorescein isothiocyanate (FITC)-conjugated secondary antibodies (Invitrogen). Coverslips were washed and mounted onto slides, and cells were visualized using a Bio-Rad MRC Scanning Confocal System (Hercules, CA).

2.7. Statistical analysis

Experiments were independently replicated a minimum of three times unless otherwise stated. Data among replicate experiments were standardized by expressing individual experiments as a fold-difference versus either control, or versus mock transfected cells. Transformed data from replicated experiments were analyzed by one-way ANOVA without including values from the control or mock transfected group (arbitrarily set to 1.0), and the Fisher's protected least significant difference multiple range test. Alternatively, in cases where a specific comparison was between two groups, original data from the replicate experiments were analyzed using a Student's *t*-test.

3. Results

3.1. Treatment with Z-LLF enhances TRAIL-induced cell death

Treatment with TRAIL (50 ng/ml) resulted in a slight, but statistically significant, reduction in viable cells compared to control cells after a 24 h culture. Pre-treatment for 2 h with the proteasome inhibitor, Z-LLF, synergistically enhanced the cytotoxicity of TRAIL in both KGN and COV434 cells (Fig. 1).

3.2. Effects of Z-LLF occur independent of caspase-8 activity

KGN and COV434 cells were pretreated for 2 h with the caspase-8 inhibitor, IETD (20 μM), prior to culture for 18 h with TRAIL (50 ng/ml), Z-LLF (10 μM, KGN; 2 μM, COV434), or a combination of Z-LLF plus TRAIL (Z-LLF added 2 h prior to TRAIL). While inhibition of caspase-8 activity reversed the effects of TRAIL, IETD failed to prevent Z-LLF-induced loss of viability (Fig. 2a). Additionally, pre-treatment with IETD prevented the synergistic effect of Z-LLF plus TRAIL-induced loss of cell viability. Notably, the caspase-9 inhibitor, LEHD, also reversed the synergistic effect of Z-LLF plus TRAIL-induced cell death (Fig. 2b).

3.3. Z-LLF increases dr5 and bax mRNA and protein levels in GCT cell lines

Following an 18 h culture of KGN and COV434 cells, DR5 and Bax protein levels were elevated in response to treatment with Z-LLF, but not with TRAIL (Fig. 3a). To establish whether the effect of Z-LLF is a transcriptionally regulated event, mRNA levels for *dr5* and *bax*

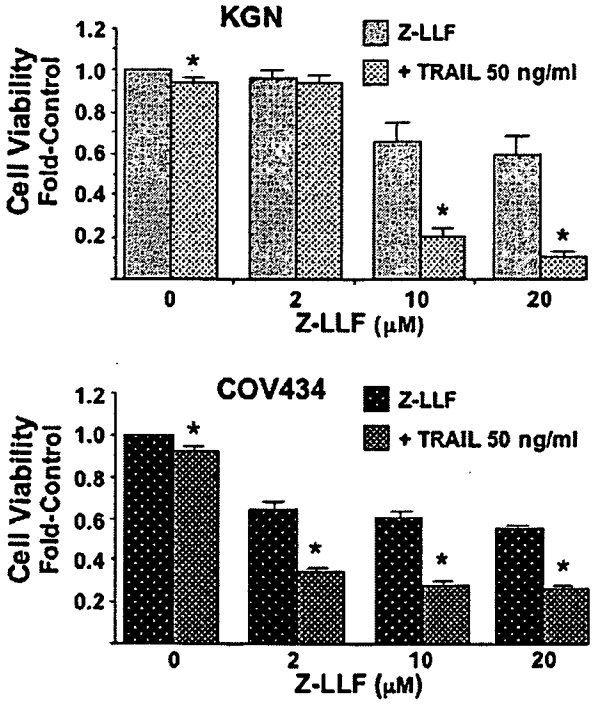

Fig. 1. Treatment of KGN and COV434 cells for 18 h with TRAIL (50 ng/ml) results in a decrease in cell viability. Pretreatment with the proteasome inhibitor, Z-LLF-CHO (Z-LLF; 2–20 μM) reduces cell viability, and synergistically reduces cell viability in the presence of TRAIL. Data are expressed as mean viability ± SEM compared to control-cultured cells. $^*p < 0.05$ by *t*-test compared to the absence of TRAIL; $n = 4$–7 replicate experiments.

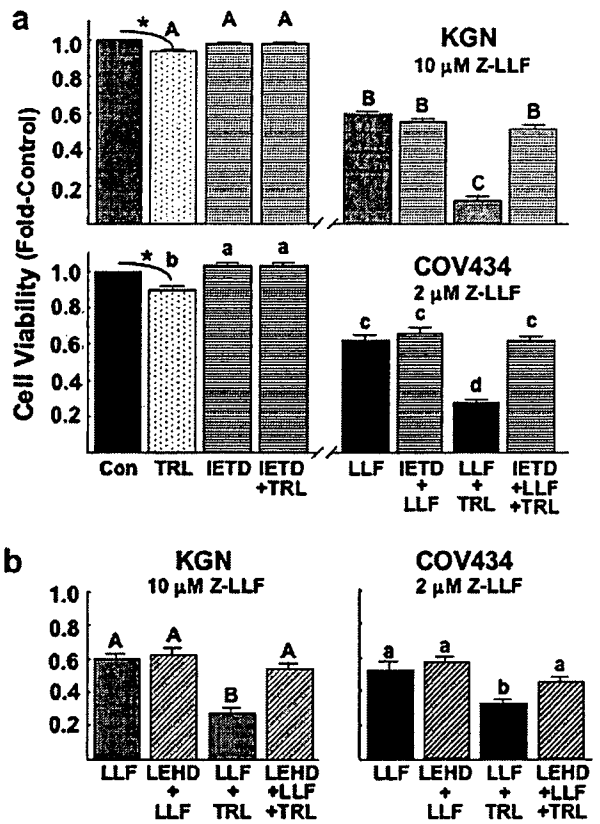

Fig. 2. (a) Pre-treatment of KGN and COV434 for 2 h with Z-IETD-FMK (IETD; 20 μM) prevents TRAIL (100 ng/ml)-and TRAIL-plus-Z-LLF-reduced cell viability, but not that induced by Z-LLF alone. $^*p < 0.05$ by *t*-test; (A–C); a–d: $p < 0.05$; $n = 5$ (KGN) or 6 (COV434) replicate experiments. (b) Pre-treatment with the capase-9 inhibitor, Z-LEHD-FMK (LEHD) does not prevent Z-LLF-induced loss of cell viability, but does reverse the combinatorial effect of TRAIL co-treated with Z-LLF. A, B; a, b: $p < 0.01$; $n = 4$ replicate experiments.

mRNA were evaluated. In both GCT lines, *dr5* and *bax* expression levels were significantly elevated over controls (Fig. 3b).

3.4. Treatment with Z-LLF promotes mitochondrial cytochrome c release in KGN cells

KGN cells were incubated with or without Z-LLF for 8 h to observe the localization of cytochrome *c* (a marker of Bax activity and apoptosis). In control KGN cells, cytochrome *c* staining was evident in mitochondria surrounding the nucleus (Fig. 3c). Following treatment with Z-LLF, immunofluorescent staining was visible throughout the cytosol and within the nucleus in cells undergoing early apoptosis (Fig. 3d). During the latter stages of apoptosis (Fig. 3e), cytochrome *c* staining was more concentrated as apoptotic cells became condensed.

3.5. Z-LLF-enhanced cell death is independent of p53

In preliminary studies we determined that both KGN and COV434 express wild-type p53 (unpublished data). Treatment with Z-LLF produced increased levels of p53 protein in both KGN and COV434 cell lines (Fig. 4a). However, this increase was not reflected at the level of transcription, as treatment of COV434 cells with Z-LLF led to a significant decrease in *p53* mRNA, and no effect in KGN cells (Fig. 4b). To further investigate whether the effects of Z-LLF on cell viability in KGN and COV434 are dependent on p53 expression, each cell line was transfected with control siRNA or sip53. Knock-down efficiency was monitored by PCR (Fig. 5a) and Western blot (Fig. 5b). In both GCT lines, transfection with sip53 had no effect on Z-LLF-induced loss of cell viability as compared to cells transfected with control siRNA (Fig. 5c and d). Finally, transfection with sip53, both in the absence and presence of Z-LLF treatment, resulted in the loss of p53 protein (Fig. 6a), yet the absence of p53 protein failed to prevent induction of *dr5* and *bax* mRNA expression following treatment with Z-LLF (Fig. 6b).

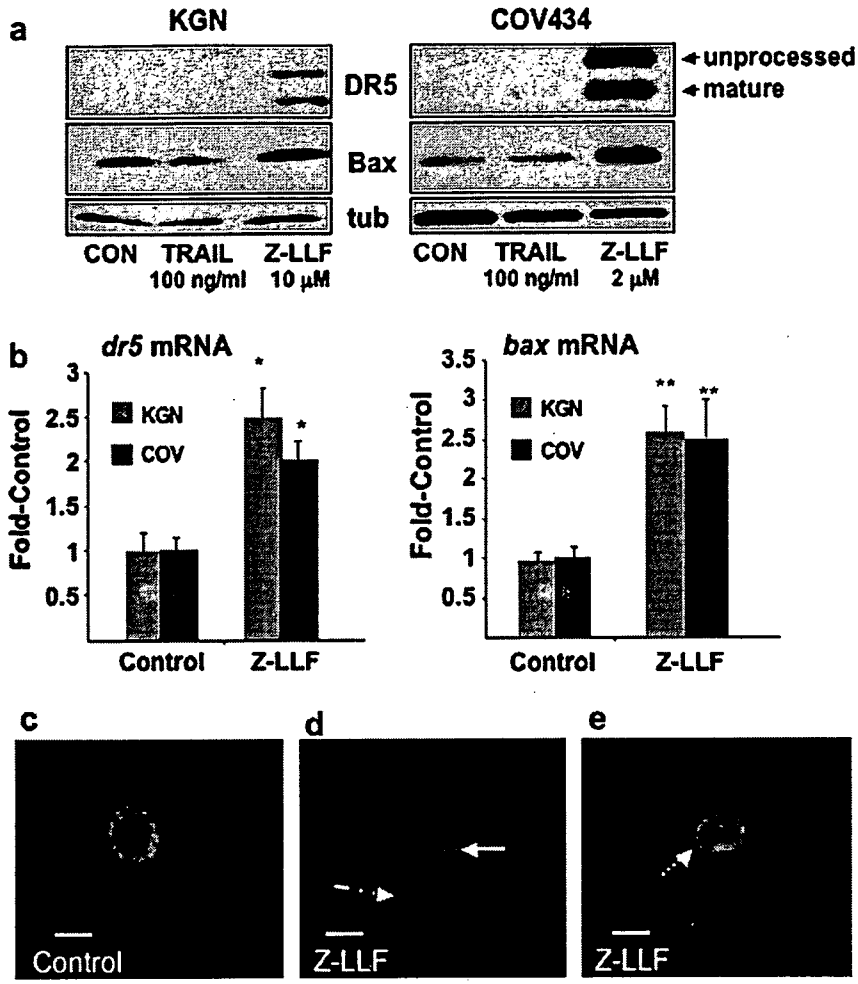

Fig. 3. (a) Western blot analysis of DR5 and Bax protein expression in KGN and COV434 cells. Culture for 18 h with Z-LLF, but not TRAIL, increases levels of DR5 (unprocessed and mature forms) and Bax protein. Representative of three replicate experiments. (b) Real-time PCR for *dr5* and *bax* mRNA expression in KGN and COV434 cells. $^{*}p < 0.01$; $^{**}p < 0.01$ versus respective control; $n = 3$ replicate experiments. (c) Immunofluorescent staining of cytochrome *c* in control KGN cells is predominantly localized to the mitochondria. (d) Following treatment for 8 h with Z-LLF (10 μM), cytochrome *c* is localized to both the cytosol (dashed arrow) and nucleus (solid arrow) during the early stages of apoptosis. (e) A cell during the latter stages of apoptosis following treatment with Z-LLF for 8 h. Cytochrome *c* becomes concentrated as entire cells become condensed (dotted arrow). Omission of primary antibody served as a control for antibody specificity, and resulted in an absence of immunofluorescence (not shown). Bar = 10 μM. Representative of three replicate experiments.

4. Discussion

The results presented herein are the first to describe the effectiveness of a proteasome inhibitor and the naturally occurring cytokine, TRAIL, to induce apoptosis in tumor cells specifically of granulosa cell origin. These data indicate that proteasome-inhibitors may be useful in treatment of GCTs, a finding that is further underscored by the ability of proteasome-inhibitors to enhance the efficacy of TRAIL treatment. Functionally, this occurs, at least in part, through the up-regulation of both the DR5 receptor and the pro-apoptotic protein, Bax, the latter of which promotes release of cytochrome *c* from the mitochondria [14]. Although multiple cell types have demonstrated that the transcriptional regulation of *dr5* and *bax* is dependent upon p53 activity [27], the present studies with KGN and COV434 GCT lines indicate that proteasome inhibitor-enhanced expression of DR5 and Bax occurs via a p53-independent pathway.

Recently, TRAIL treatment was shown to increase the efficacy of proteasome inhibitor-induced cell death in both TRAIL-resistant and -sensitive hOSE cell lines [28]. Likewise, while both GCT cell lines examined herein demonstrate a slight, but significant, loss of viability in response to treatment with TRAIL after an 18 h culture,